International Journal of Bifurcation and Chaos

VIBRATION DYNAMICS OF AN INCLINED CABLE EXCITED NEAR ITS SECOND NATURAL FREQUENCY

VASSIL V. TZANOV
Department of Engineering Mathematics, University of Bristol
Queen's Building, University Walk, Bristol BS8 1TR, United Kingdom
vassiltzanov@gmail.com

BERND KRAUSKOPF
Department of Mathematics, The University of Auckland
Private Bag 92019, Auckland 1142, New Zealand
b.krauskopf@auckland.ac.nz

SIMON A. NEILD
Department of Mechanical Engineering, University of Bristol
Queen's Building, University Walk, Bristol BS8 1TR, United Kingdom
simon.neild@bristol.ac.uk

Received (to be inserted by publisher)

Inclined cables are essential structural elements that are used most prominently in cable stayed bridges. When the bridge deck oscillates due to an external force, such as passing traffic, cable vibrations can arise not only in the plane of excitation but also in the perpendicular plane. This undesirable phenomenon can be modelled as an auto-parametric resonance between the in-plane and out-of-plane modes of vibration of the cable. In this paper we consider a three-mode model, capturing the second in-plane, and first and second out-of-plane modes, and use it to study the response of an inclined cable that is vertically excited at its lower (deck) support at a frequency close to the second natural frequency of the cable. Averaging is applied to the model and then the solutions and bifurcations of the resulting averaged differential equations are investigated and mapped out with numerical continuation. In this way, we present a detailed bifurcation study of the different possible responses of the cable. We first consider the equilibria of the averaged model, of which there are four types that are distinguished by whether each of the two out-of-plane modes is present or not in the cable response. Each type of equilibrium is computed and represented as a surface over the plane of amplitude and frequency of the forcing. The stability of the equilibria changes and different surfaces meet along curves of bifurcations, which are continued directly. Overall, we present a comprehensive geometric picture of the two-parameter bifurcation diagram of the constant-amplitude coupled-mode response of the cable. We then focused on bifurcating periodic orbits, which correspond to cable dynamics with varying amplitudes of the participating second in-plane and second out-of-plane modes. The range of excitation amplitude and frequency is determined where such whirling cable motion can occur. Further bifurcations — period-doubling cascades and a Shilnikov homoclinic bifurcation — are found that lead to a chaotic cable response. Whirling and chaotic cable dynamics are confirmed by time-step simulations of the full three-mode model. The different cable responses are characterized, and can be distinguished clearly, by the their motion at the quarter-span and by their frequency spectra.

Keywords: Cable dynamics, parametric excitation, modal equations, bifurcation analysis, equilibrium surfaces, quasi-periodic and chaotic cable motion.

1. Introduction

In a cable-stayed bridge, the towers support the deck by many inclined cables of different length. Deck motion due to traffic or other external forces can excite one or several of the inclined cables [Irvine, 1981]. The cable dynamics itself is nonlinear, owing to gravitational sag and tension variations during oscillations. These nonlinearities result in the coupling between different basic modes of the cable. Interesting nonlinear dynamics may arise due to this coupling, and in light of the following important properties of the system:

(1) cables are very lightly damped;
(2) the resonant frequencies of a cable are near or exact integer multiples of each other;
(3) both in-plane (vertical) and out-of-plane (sway) motion is possible;
(4) many different lengths of cable are present and so it is likely that the fundamental frequency of the bridge deck is very close to the resonant frequency of at least one of the cables.

From a practical point of view, motion of the cables is an unwanted phenomenon. Understanding the underlying nonlinear dynamics is crucial for designing effective measures to mitigate large amplitude cable responses and motivates much of the research in the field.

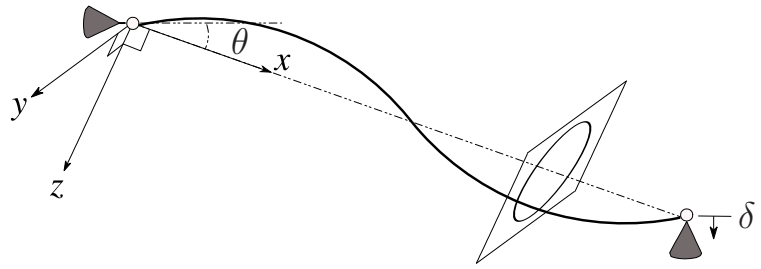

Fig. 1. Schematic representation of a cable with incline θ and vertical input motion δ at the lower attachment point; shown is the case of a non-planar whirling response with fixed middle point and an ellipse-like trace in the quarter-span plane. Here $x \in [0, \ell]$ is the position along the cable, where ℓ is the support separation distance, while the z-axis and the y-axis define the in-plane and out-of-plane directions of the cable, respectively.

This paper is concerned with the underlying basic issue — the motion of a single harmonically excited inclined cable. Specifically, we consider here an inclined cable that is subject to harmonic vertical excitation of its lower support at a frequency close to its second natural frequency; the corresponding physical setup is sketched in Fig. 1. Note that we use the term *mode* throughout to refer to a mode of the linearised cable dynamics; see for example [Nayfeh & Pai, 2004]. It has been shown that small amplitude motion of the cable anchorage can result in large amplitude cable vibrations [Nayfeh & Pai, 2004]. The main question is when and how the different modes of the cable are excited as a function of excitation frequency and amplitude.

The dynamics of an inclined cable has been investigated in the literature in different ways. Considering just the in-plane response, [Lilien & Pinto Da Costa, 1994] showed that parametric excitation of modes is most significant when the ratio between the excitation frequency and the natural frequency of the cable is at or near $2:1$. More generally, however, both in-plane and out-of-plane modes must be considered [Srinil *et al.*, 2004]. For example, [Georgakis *et al.*, 2001] considered multiple in-plane and out-of-plane modes for the case where auto-parametric resonance and cable nonlinearities are included. Using Mathieu-type equations to model auto-parametric resonance [Tagata, 1977; Uhrig, 1993] also capture coupling between the in-plane and out-of-plane modes of vibration [Fujino *et al.*, 1993; Gattulli *et al.*, 2005, 2004]. The loss of stability of the semi-trivial solution, for which the response is limited to just the directly excited mode, has also been studied in detail [Berlioz &Lamarque, 2005; Gonzalez-Buelga *et al.*, 2008; Macdonald *et al.*, 2010; Rega, 2004a,b; Rega *et al.*, 1999]. Experimental analysis of the cable response in out-of-plane modes due to vertical excitation have been reported in [Rega *et al.*, 1997; Rega & Alaggio, 2009; Rega *et al.*, 2008].

Related is research into the vibrations of a string, but here the effects of inclination and gravitational sag do not play a role. The nonlinear equation of motion of a string go back to [Kirchhoff, 1883], and the simplest model for the transverse vibration of a string, which involves motion in one plane only, yields a forced damped Duffing equation; see [Narashima, 1968]. The general equations of coupled modes from [Narashima, 1968] are reduced in [Miles, 1984] and in [Bajaj & Johnson, 1992; Johnson & Bajaj, 1989] to a set of four averaged ODEs for the amplitudes of the basic horizontal and the vertical modes, which shares many features with the one developed by O'Reilly and Holmes [O'Reilly & Holmes, 1992] who use a different scaling. In vibrating strings also more complicated motion has been observed. [Miles, 1984] mentions quasi-periodic responses and the possibility of a chaotic response, and [Bajaj & Johnson, 1992; Johnson & Bajaj, 1989] found them in numerical simulations. [Molteno & Tufillaro, 1990] as well as [O'Reilly & Holmes, 1992] found quasi-periodic and chaotic string responses experimentally. Recently, [Molteno & Tufillaro, 2004] conducted an experiment that again showed a quasi-periodic string response.

Our object of study is the three-mode model from [Gonzalez-Buelga *et al.*, 2008] of an inclined cable that is vertically excited near its second natural frequency. The model takes the form of a periodically forced system of three second-order differential equations for the coupled nonlinear dynamics of the directly excited second in-plane mode and the auto-parametrically forced first and second out-of-plane modes. After scaling and averaging one obtains a system of six autonomous ordinary differential equations. Their solutions represent the coefficients that modulate the sine and cosine members in the mode shape functions of the cable response. Hence, steady-state solutions (equilibria) of the averaged system correspond to periodic dynamics of the cable at the forcing frequency, and periodic solutions of the avaraged system correspond to quasi-periodic or locked two-frequency dynamics of the cable. The model from [Gonzalez-Buelga *et al.*, 2008] is based on general equations of motion that [Warnitchai *et al.*, 1995] derived for the nonlinearly coupled basic modes of an inclined cable subject to support excitation; see [Wagg & Neild, 2010] for an extended discussion of its derivation.

In [Gonzalez-Buelga *et al.*, 2008] the three-mode model was used to identify the boundary — in the plane of frequency and amplitude of the forcing — of the directly excited pure second in-plane response; this was achieved via the examination of the local stability of each out-of-plane mode about its zero response, and these results were validated with experimental data of a scaled model of an inclined cable. This experimental work was extended to excitation close to other natural frequencies in [Macdonald *et al.*, 2010]; moreover, these authors provided generalised equations of Warnitchai type for excitation at every natural frequency and responses in all possible modes. [Marsico *et al.*, 2011] investigated a four-mode model of this type, which also includes the first in-plane mode to allow for a wider range of forcing frequencies around the second natural frequency; the response amplitudes of the various modes were studied theoretically and compared with experimental measurements for the same cable that was used in [Macdonald *et al.*, 2010].

In this paper we perform a detailed bifurcation study of the three-mode model from [Gonzalez-Buelga *et al.*, 2008] (introduced in Sec. 2 below) of an inclined cable of length L with second natural frequency ω_2 for both in-plane and out-of-plane vibrations. The cable is excited vertically at its lower end by the periodic excitation $\delta = \Delta\cos(\Omega t)$, where Ω is near ω_2. Specifically, we

(1) present a complete and geometric picture of when and how the two basic out-of-plane modes contribute to the periodic cable response; and
(2) identify regions in parameter space where quasi-periodic and chaotic cable dynamics can be found.

To this end, we first investigate the four different types of equilibria of the averaged equations, which are distinguished by which of the two out-of-plane modes contribute to the cable response (i.e., have non-zero amplitudes). These equilibria and their bifurcations are continued with the numerical continuation software AUTO [Doedel *et al.*, 2000; Doedel, 2007], where the frequency ratio Ω/ω_2 and the dimensionless amplitude Δ/L are the continuation parameters. This allows us to compute and represent the different equilibria as surfaces in $(\Omega/\omega_2, \Delta/L, ||N||)$-space, where $||N||$ is a suitable norm of the amplitude contributions of the different basic modes. Stable equilibria correspond to observable periodic responses of the cable, and they are distinguished by darker shading of the respective surface. The different surfaces meet or encounter changes of stability along curves of saddle-node (fold), branching and Hopf bifurcations, which are computed

directly with AUTO. The surfaces of the different types of equilibria are introduced one by one, culminating in an overall comprehensive geometric picture of connected surfaces that catalogues the overall periodic cable dynamics. Importantly, we find considerable regions of stability for each of the possible multi-mode responses. These results vastly extend what was known about the steady-state solutions structure of the three-mode model from [Gonzalez-Buelga *et al.*, 2008], and they allow one to identify the contributions of the three basic in-plane and out-of-plane modes to the observed periodic cable response for given (or changing) amplitude and frequency of the periodic excitation $\delta(t)$. This is illucidated with one-parameter bifurcation diagrams at cross sections of interest.

We then study periodic orbits of the averaged equations that correspond to a cable response with varying amplitudes of the contributing second in-plane and second out-of-plane modes, while the first out-of-plane mode is not excited. We find further bifurcations, including period-doubling cascades and a Shilnikov homoclinic bifurcation, as well as associated chaotic cable dynamics. Regions where these solutions can be found are identified in the $(\Omega/\omega_2, \Delta/L)$-plane. The existence of these new types of solutions is verified with simulations of the full three-mode model; they can be distinguished clearly by their quarter-span traces and frequency spectra.

The paper is organized as follows. Section 2 introduces the model describing the evolution of the three basic modes of the cable, its averaged version and the specific choices for the parameters of the cable. Section 3 is devoted to the bifurcation analysis of equilibria of the averaged system, which are solutions of the full three-mode model with constant amplitudes of the contributing coupled basic three modes. The surfaces of the four different types of equilibria are introduced in Secs. 3.1 to 3.4 to yield the overall bifurcation diagram presented in Secs. 3.5 and 3.6. Section 4 is concerned with varying-amplitude responses of the cable. In Sec. 4.1 we perform a one-parameter study in Δ/L of the periodic orbits that bifurcate from Hopf bifurcations of the constant-amplitude response with contributions from the second in-plane and out-of-plane modes. How these solutions manifest themselves in terms of the observed cable dynamics is discussed in Sec. 4.2. In Sec. 4.3 we consider the influence of Ω/ω_2 on the one-parameter bifurcation diagram and show that Shilnikov homoclinic orbits exist, and in Sec. 4.4 we present the regions in the $(\Omega/\omega_2, \Delta/L)$-plane where the different types of varying-amplitude responses of the cable can be found. Finally, we draw some conclusion in Sec. 5.

2. Three-Mode Model of Inclined Cable Dynamics

We consider an inclined cable excited near its second natural frequency via vertical motion of its lower support; see Fig. 1. The cable analysed is a 1.98m long and 0.8mm diameter steel cable, inclined at 20^o to the horizontal, with a mass of 0.67 kg/m. It is a scaled model of a realistic cable-stayed bridge cable and matches the one experimentally tested in [Gonzalez-Buelga *et al.*, 2008]. To analyse the cable dynamics we consider the directly excited second in-plane mode z_2 with natural frequency $\omega_2 = 2\omega_1$, and the first and second out-of-plane modes y_1 and y_2 with natural frequencies ω_1 and ω_2, respectively. These two out-of-plane modes are included as they have $2:1$ and $1:1$ internal resonances with the second in-plane mode. Note that the first in-plane mode is not included here as its frequency is $1.07\,\omega_1$ (see [Gonzalez-Buelga *et al.*, 2008]) and so only exhibits a significant response at excitation frequencies that are further away from the second in-plane mode than those we focus on here.

The equations of motion we use are the modal equations derived by [Warnitchai *et al.*, 1995], who performed a Galerkin decomposition based on the mode shapes of the linear equivalent system; see [Wagg & Neild, 2010] for an in-depth discussion of this derivation. The derivation of the Warnichai equations for the three modes y_1, y_2 and z_2 taken into account here (which are independent of the distance x along the cable) yield the periodically forced, nonautonomous system of second-order ODEs

$$\begin{cases} \ddot{y}_1 + 2\xi\omega_1\dot{y}_1 + \omega_1^2 y_1 + \frac{W_{12}y_1^3}{4} + W_{12}y_1(y_2^2+z_2^2) + N_1\delta y_1 = 0, \\ \ddot{y}_2 + 2\xi\omega_2\dot{y}_2 + \omega_2^2 y_2 + W_{12}y_2y_1^2 + 4W_{12}y_2(y_2^2+z_2^2) + 4N_1\delta y_2 = 0, \\ \ddot{z}_2 + 2\xi\omega_2\dot{z}_2 + \omega_2^2 z_2 + W_{12}z_2y_1^2 + 4W_{12}z_2(y_2^2+z_2^2) + 4N_1\delta z_2 = B\ddot{\delta}, \end{cases} \tag{1}$$

were $\delta = \Delta\cos(\Omega t)$ is the lower support vertical excitation. The out-of-plane and in-plane natural frequen-

Table 1. Cable parameters and their values; note that B and ξ are nondimensional.

N_1 [Hz^2/m]	W_{12} [s^{-2}m^{-2}]	ω_1 [rad/s]	B	ξ
5.6×10^4	9.46×10^5	27.7	0.2991	0.002

cies ω_1 and ω_2 of the linearised system are given by

$$\omega_n = \frac{n\pi}{\ell}\sqrt{\frac{\sigma_s}{\rho}}, \tag{2}$$

where ℓ is the support separation distance; see Fig. 1. Moreover, ξ is the damping ratio and it is assumed to be the same for all three basic modes, which is in line with the experimental study; its value and that of the fixed parameters W_{12}, N_1 and B that relate to the cable's physical properties are given in Table 1; see [Gonzalez-Buelga *et al.*, 2008] for the details.

From the Warnichai equations (1) one can derive equations for the amplitude dynamics of the three modes. To this end, the solutions are written in the form

$$\begin{aligned} y_i &= y_{ic}\cos(\omega_i\tau) + y_{is}\sin(\omega_i\tau), \qquad i \in 1,2, \\ z_2 &= z_{2c}\cos(\omega_2\tau) + z_{2s}\sin(\omega_2\tau). \end{aligned} \tag{3}$$

Then scaling and averaging is applied to yield the system

$$\begin{cases} y_{1c}' = -\xi\omega_1 y_{1c} - \left(\mu\omega_1 + \frac{N_1\Delta}{4\omega_1} - \frac{3W_{12}}{32\omega_1}Y_1^2 - \frac{W_{12}}{4\omega_1}(Y_2^2+Z_2^2)\right)y_{1s}, \\ y_{1s}' = \left(\mu\omega_1 - \frac{N_1\Delta}{4\omega_1} - \frac{3W_{12}}{32\omega_1}Y_1^2 - \frac{W_{12}}{4\omega_1}(Y_2^2+Z_2^2)\right)y_{1c} - \xi\omega_1 y_{1s}, \\ y_{2c}' = \left(\frac{W_{12}z_{2c}z_{2s}}{2\omega_1} - 2\xi\omega_1\right)y_{2c} - \left(2\mu\omega_1 - \frac{W_{12}}{8\omega_1}\left(Y_1^2 + 6(Y_2^2+Z_2^2) - 4z_{2c}^2\right)\right)y_{2s}, \\ y_{2s}' = \left(2\mu\omega_1 - \frac{W_{12}}{8\omega_1}\left(Y_1^2 + 6(Y_2^2+Z_2^2) - 4z_{2s}^2\right)\right)y_{2c} - \left(2\xi\omega_1 + \frac{W_{12}z_{2c}z_{2s}}{2\omega_1}\right)y_{2s}, \\ z_{2c}' = \left(\frac{W_{12}y_{2c}y_{2s}}{2\omega_1} - 2\xi\omega_1\right)z_{2c} - \left(2\mu\omega_1 - \frac{W_{12}}{8\omega_1}\left(Y_1^2 + 6(Y_2^2+Z_2^2) - 4y_{2c}^2\right)\right)z_{2s}, \\ z_{2s}' = \left(2\mu\omega_1 - \frac{W_{12}}{8\omega_1}\left(Y_1^2 + 6(Y_2^2+Z_2^2) - 4y_{2s}^2\right)\right)z_{2c} - \left(2\xi\omega_1 + \frac{W_{12}y_{2c}y_{2s}}{2\omega_1}\right)z_{2s} - B\Delta\omega_1. \end{cases} \tag{4}$$

Here the scaled time $\tau = (1+\mu)t$ is used, where μ is the frequency detuning of $\Omega = \omega_2(\mu+1)$, the prime denotes differentiation with respect to τ, and

$$\begin{aligned} Y_i &= \sqrt{y_{ic}^2 + y_{is}^2}, \qquad i \in 1,2, \\ Z_2 &= \sqrt{z_{2c}^2 + z_{2s}^2} \end{aligned}$$

represent the amplitudes of the three modes, respectively. More details of the scaling and averaging procedure applied to the Warnichai equations can be found in [Gonzalez-Buelga *et al.*, 2008; Tzanov, 2012].

Equations (4) are a system of six autonomous ODEs and, hence, their solutions and bifurcations can be followed by means of numerical continuation; we use the software package AUTO [Doedel *et al.*, 2000; Doedel, 2007] for this purpose. In our bifurcation study we use the normalized amplitude Δ/L and the

frequency Ω/ω_2 of the excitation as the continuation parameters. Numerical simulations of the Warnitchai equations (1) and its averaged version (4) have been shown to agree well over the range

$$\Delta/L \in [0, 3.5\times10^{-3}], \quad \Omega/\omega_2 \in [0.95, 1.05]; \tag{5}$$

see [Gonzalez-Buelga *et al.*, 2008]. Moreover, we checked that, if the first in-plane mode is actually included, its effects are only noticeable for $\Omega/\omega_2 > 1.04$. The range (5) of excitation amplitude and frequency around ω_2 may appear to be quite small. However, these quantities have been scaled and it was demonstrated in [Gonzalez-Buelga *et al.*, 2008; Marsico *et al.*, 2011] that (5) is the physically relevant range of nonlinear resonance of the cable, which is fully accessible and resolvable experimentally. As part of our bifurcation study we consider the slightly extended range of Ω/ω_2 up to 1.07. The reason is that this allows us to detect solutions for larger Ω/ω_2 that are then continued back to the range (5), where their validity is not in doubt; such solutions might otherwise be overlooked.

As the lower cable support is excited vertically at a frequency close to ω_2, from linear dynamics we expect the cable response to be a standing wave in the vertical plane with a sinusoidal shape and fixed mid-span point. These dynamics correspond in equations (4) to an equilibrium with a contribution from the basic in-plane mode only (i.e., $Y_1 = Y_2 = 0$); we refer to this equilibrium as the pure Z_2-response. Due to the nonlinear behaviour of the cable, beyond certain excitation amplitude and frequency boundaries the pure Z_2-response ceases to be stable. At such boundaries one or both of the out-of-plane modes will start to contribute to the dynamics of the cable, and this corresponds to the emergence of stable equilibria of (4) with non-zero contributions from Y_1 and Y_2. Note, however, that, because it is directly excited, the basic in-plane mode will always contribute to the dynamics (that is, Z_2 is always non-zero in the presence of excitation). As is usual in the field, we plot solutions in terms of the norm

$$||N|| = \frac{\sqrt{Z_2^2 + Y_1^2 + Y_2^2}}{L}, \tag{6}$$

which represents the combined amplitude of the cable response associated with the (steady-state) solutions of (4).

3. Bifurcation Analysis of the Constant-Amplitude Response

We now present a geometric picture of how the different possible equilibrium solutions of (4) depend on the amplitude Δ/L and the frequency Ω/ω_2 of the excitation. These equilibria correspond to the constant-amplitude responses of the full Warnichai equations (1). The task is to find an overall consistent bifurcation diagram of the equilibria of (4), their stability and bifurcations. To this end, we represent the equilibria of the system as surfaces in $(\Omega/\omega_2, \Delta/L, ||N||)$-space. The starting point is the trivial equilibrium for $\Delta/L = 0$ (with zero contribution from all modes) for a fixed frequency Ω/ω_2 close to unity; continuation in Δ/L then allows us to follow the branch of the pure Z_2-response (with zero contributions from Y_1 and Y_2). This branch is initially stable but loses stability in different types of bifurcations, where equilibria with contributions from the Y_1-mode and/or the Y_2-mode emerge. We find and consider the following types of equilibria:

(1) the pure Z_2-response with a contribution from only the in-plane mode (where $Y_1 = Y_2 = 0$); curves and the surface of the pure Z_2-response are denoted $\mathcal{L}$.
(2) the coupled (Z_2, Y_1)-response with contributions from the second in-plane mode and the first out-of-plane mode (where $Y_2 = 0$); curves and the surface of the coupled (Z_2, Y_1)-response are denoted $\mathcal{L}_1$.
(3) the coupled (Z_2, Y_2)-response with contributions from the second in-plane mode and the second out-of-plane mode (where $Y_1 = 0$); curves and the surface of the coupled (Z_2, Y_2)-response are denoted $\mathcal{L}_2$.
(4) the coupled (Z_2, Y_1, Y_2)-response with contributions from all three basic modes; curves and the surface of the coupled (Z_2, Y_1, Y_2)-response are denoted $\mathcal{L}_{12}$.

The surfaces of these four different types of equilibria are constructed one by one in $(\Omega/\omega_2, \Delta/L, ||N||)$-space from continuation runs in Δ/L for suitably many fixed choices of Ω/ω_2. The rendering of the surface images in this paper is performed with Matlab. Curves of bifurcations are computed by two-parameter

continuations and then also plotted in $(\Omega/\omega_2, \Delta/L, ||N||)$-space, where they lie on corresponding surfaces of equilibria. We find branching, fold (saddle-node) and Hopf bifurcations as follows:

B_1 denotes a branching bifurcation where $\mathcal{L}_1$ bifurcates from $\mathcal{L}$;
B_2 denotes a branching bifurcation where $\mathcal{L}_2$ bifurcates from $\mathcal{L}$;
B_{12}^1 denotes a branching bifurcation where $\mathcal{L}_{12}$ bifurcates from $\mathcal{L}_1$;
B_{12}^2 denotes a branching bifurcation where $\mathcal{L}_{12}$ bifurcates from $\mathcal{L}_2$;

F_{Z_2} denotes a fold bifurcation of $\mathcal{L}$;
F_{Y_1}, F'_{Y_1} and F''_{Y_1} denote fold bifurcations of $\mathcal{L}_1$;
F_{Y_2} denotes a fold bifurcation of $\mathcal{L}_2$;
$F_{Y_{12}}$ and $F^1_{Y_{12}}$ denote fold bifurcations of $\mathcal{L}_{12}$;

H_2 denotes a Hopf bifurcation of $\mathcal{L}_2$;
H_{12} denotes a Hopf bifurcation of $\mathcal{L}_{12}$.

3.1. *The surface $\mathcal{L}$ of the pure Z_2-response*

Figures 2(a) and 3(a) show two different views of the surface $\mathcal{L}$ of the pure Z_2-response in $(\Omega/\omega_2, \Delta/L, ||N||)$-space; also shown are two sets of cross sections that display the corresponding bifurcation diagram for different fixed values of Δ/L [see Figs. 2(b) and 2(c)] and Ω/ω_2 [see Figs. 3(b) and 3(c)]. Notice how the surface $\mathcal{L}$ is folded along the fold bifurcation curve F_{Z_2}. The dark blue part of $\mathcal{L}$ corresponds to the pure Z_2-response being stable; this stability region is a single region that is bounded by F_{Z_2} and the respective parts of two branch bifurcation curves B_1 and B_2. The stable pure Z_2-response corresponds to standing waves of the cable.

Figure 2(a) shows a view of the surface $\mathcal{L}$ with two intersection curves for fixed Δ/L on it, for $\Delta/L = 0.3{\times}10^{-5}$ and $\Delta/L = 7{\times}10^{-5}$, respectively. These curves represent the corresponding cross sections through $\mathcal{L}$, which are one-parameter bifurcation diagrams of the pure Z_2-response as a function of the excitation frequency Ω/ω_2; they are plotted in the $(\Omega/\omega_2, ||N||)$-plane in panels (b) and (c). Figure 2(b) shows that for sufficiently small Δ/L the resonant peak of the pure Z_2-response is what one would expect for a linear system: there is a clear peak near 1, the pure Z_2-response is a function of Ω/ω_2, and it is stable throughout. However, as the excitation amplitude Δ/L is increased the Z_2-response becomes nonlinear. Figure 2(c) is for $\Delta/L = 7{\times}10^{-5}$ and the resonance peak is now considerably bent to the right, resulting in an S-shaped curve with two fold points. However, there is practically no bi-stability, because the pure Z_2-response loses its stability at a branching bifurcation point B_2 when Ω/ω_2 is increased. The pure Z_2-response actually regains stability at a the second branching bifurcation point labelled B_2, only to lose its stability immediately at the fold point F_{Z_2}, which is virtually indistinguishable from B_2 in Fig. 2(c).

Figure 3(a) shows the surface $\mathcal{L}$ from a different view point, this time with two intersection curves for fixed excitation frequency Ω/ω_2. Panel (b) shows the intersection of $\mathcal{L}$ for $\Omega/\omega_2 = 0.97$ in the $(\Delta/L, ||N||)$-plane, where the pure Z_2-response is a monotonically increasing curve; it is stable for sufficiently small Δ/L and then loses stability at the branching bifurcation point B_1. Figure 3(c) shows the pure Z_2-response in the $(\Delta/L, ||N||)$-plane for $\Omega/\omega_2 = 1.03$. Because the curve F_{Z_2} is now intersected, the branch of the pure Z_2-response now has a characteristic S-shape. Stability is lost at the first (right) fold point along the branch. The branch turns around and effectively remains unstable throughout, except for a tiny interval of Δ/L values just past the second (left) fold point. When Δ/L is increased from zero excitation in an experiment, one first observes a pure Z_2-response until the fold point is reached and the system transitions to a different, as yet unknown, solution.

Projecting the surface $\mathcal{L}$ of the pure Z_2-response in Figs. 2(a) and 3(a) onto the $(\Omega/\omega_2, \Delta/L)$-plane gives the two-parameter bifurcation diagram in Fig. 4. It shows that for any value of Ω/ω_2 the pure Z_2-response is stable for sufficiently small Δ/L (dark blue region); see also [Gonzalez-Buelga *et al.*, 2008]. Stability of the pure Z_2-response is lost for increasing Δ/L when the solid parts of the bifurcation curves B_1 and B_2 and F_{Z_2} are crossed; such a loss of stability means that Y_1 and/or Y_2 develop a non-zero amplitude. The inset of Fig. 4, which is an enlargement near $\Omega/\omega_2 = 1$, shows that there is a cusp bifurcation point C on the fold curve F_{Z_2}; moreover, the two curves B_1 and B_2 of branching bifurcations interact at point N where

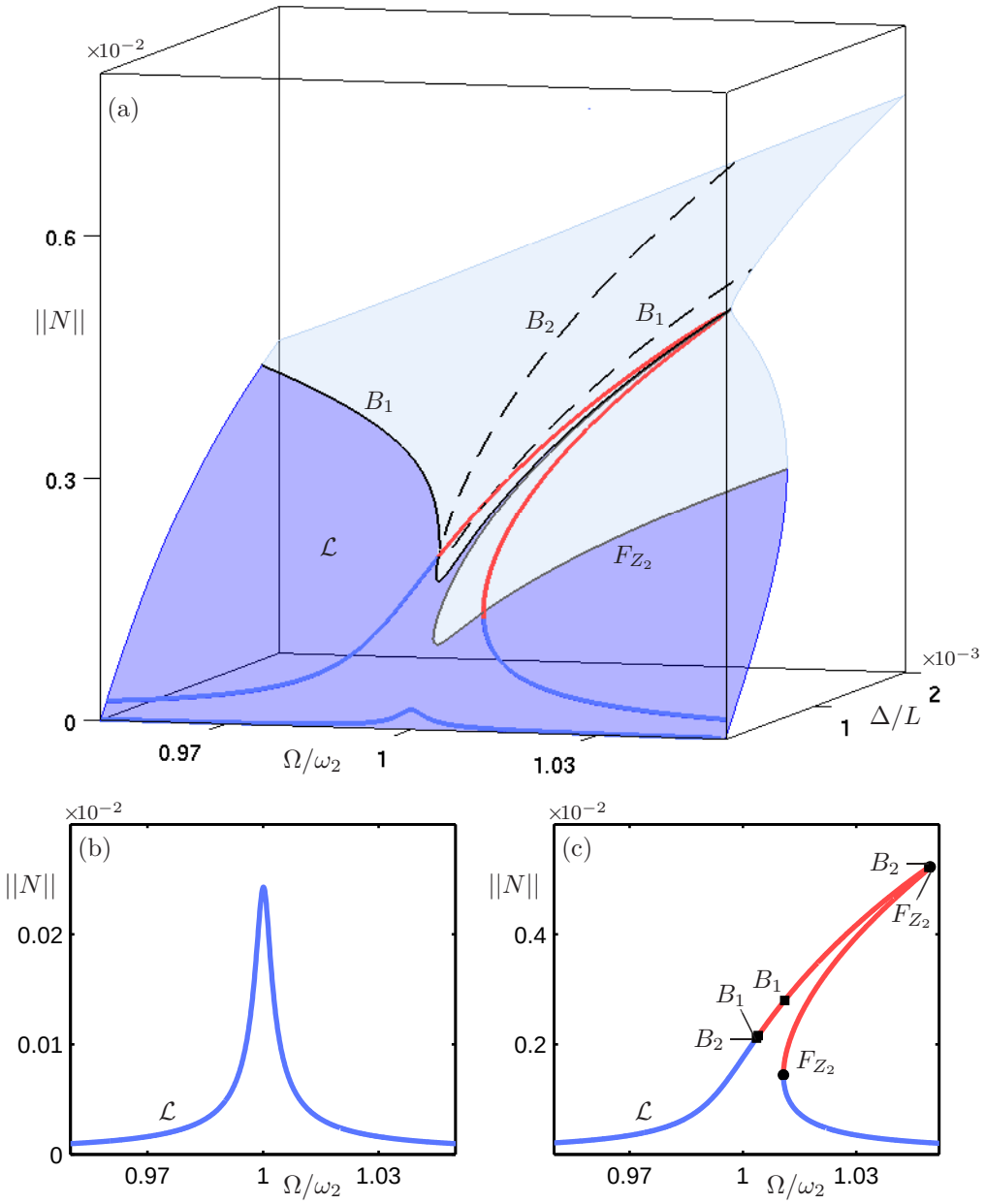

Fig. 2. Panel (a) shows the surface $\mathcal{L}$ of the pure Z_2-response of (4) in $(\Omega/\omega_2, \Delta/L, ||N||)$-space. Also shown on $\mathcal{L}$ are the branching bifurcation curves B_1, B_2 and the fold bifurcation curve F_{Z_2}; the pure Z_2-response is stable in the dark blue part and unstable in the light blue part of $\mathcal{L}$. Panels (b) and (c) show the one-parameter bifurcation diagrams in the $(\Omega/\omega_2, ||N||)$-plane for $\Delta/L = 0.3\times10^{-5}$ and for $\Delta/L = 7\times10^{-5}$, respectively; the corresponding curves are highlighted on the surface $\mathcal{L}$. Branching bifurcation points are denoted by squares and fold points by dots; the pure Z_2-response is stable along the blue parts of curves and unstable along the red parts of curves.

they exchange their roles as stability boundary for the pure Z_2-response. This means that, when Δ/L is increased the pure Z_2-response loses stability in different ways depending on the value of Ω/ω_2. For fixed $\Omega/\omega_2 < 1.003$, the frequency at which point C is located, the branching bifurcation curve B_1 is crossed and Y_1 gradually becomes nonzero. For $\Omega/\omega_2 > 1.003$, the upper part of the fold point curve F_{Z_2} (with Δ/L above the cusp point C) is crossed, which leads to a transition to quite different dynamics, where Z_2, Y_1 and Y_2 all contribute. As the inset of Fig. 4 shows, the stability region of the pure Z_2-response extends (from

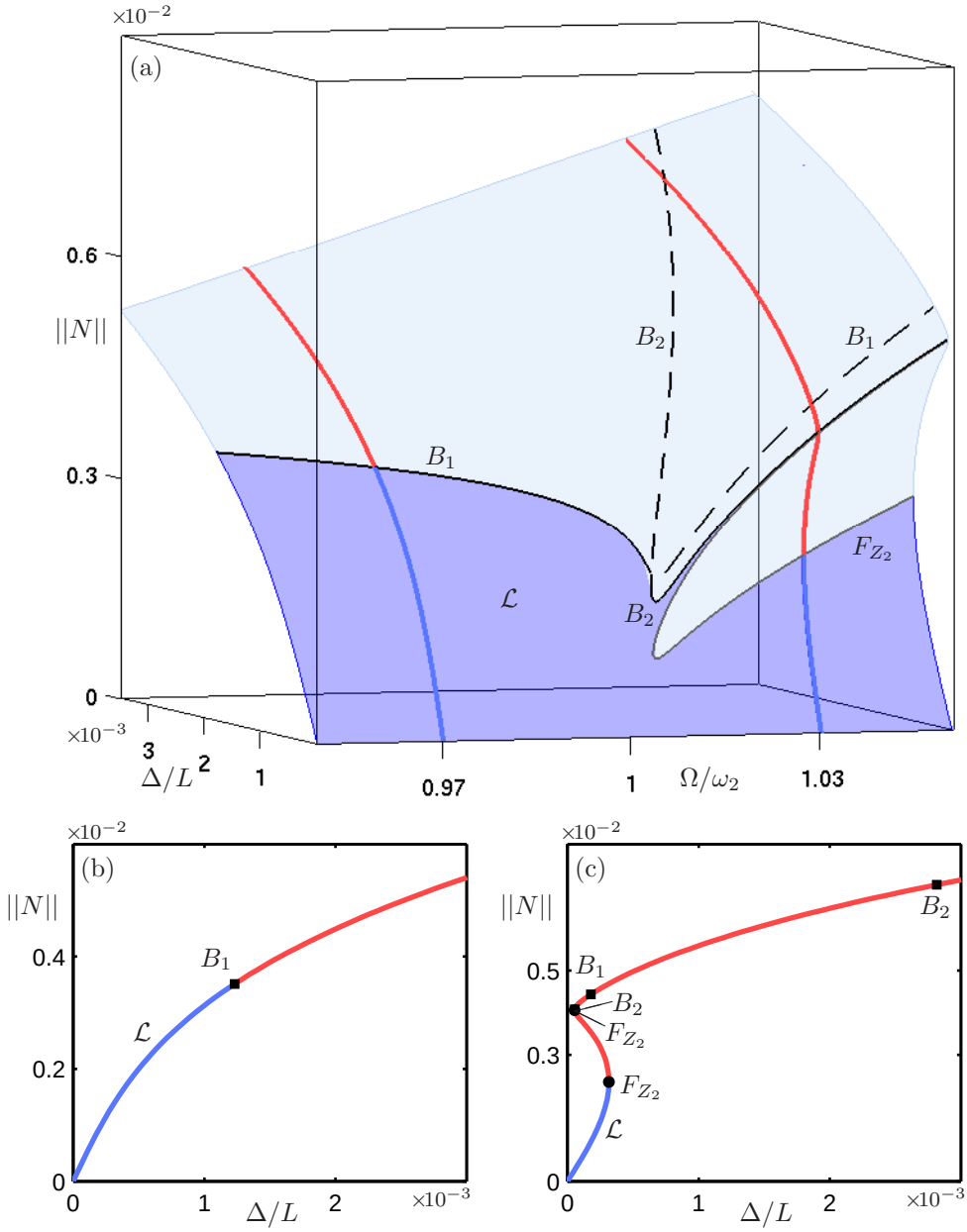

Fig. 3. Panel (a) shows a different view of the surface $\mathcal{L}$ of the pure Z_2-response; compare with Fig. 2(a). Panels (b) and (c) show the one-parameter bifurcation diagrams in the $(\Delta/L, ||N||)$-plane for $\Omega/\omega_2 = 0.97$ and for $\Omega/\omega_2 = 1.03$, respectively; the corresponding curves are highlighted on the surface $\mathcal{L}$ in panel (a).

between the points C and N) as a very thin tongue that is bounded by the curve B_2 and the lower part of the fold curve F_{Z_2} (with Δ/L above the cusp point C). When B_2 is crossed Y_2 gradually becomes nonzero; when the lower part of F_{Z_2} is crossed there is a transition to another stable pure Z_2-response (of lower amplitude). Hence, this thin tongue constitutes a region of bi-stability of the pure Z_2-response. Note that this tongue is visible much more clearly in the lifted images in $(\Omega/\omega_2, \Delta/L, ||N||)$-space of Figs. 2(a) and 3(a), which highlights the usefulness of this representation. Indeed, to understand the response of the cable for values of Ω/ω_2 where the pure Z_2-response is unstable one needs to consider the surface of bifurcating equilibria with non-trivial contributions from Y_1 and/or Y_2, which are discussed in the subsequent sections.

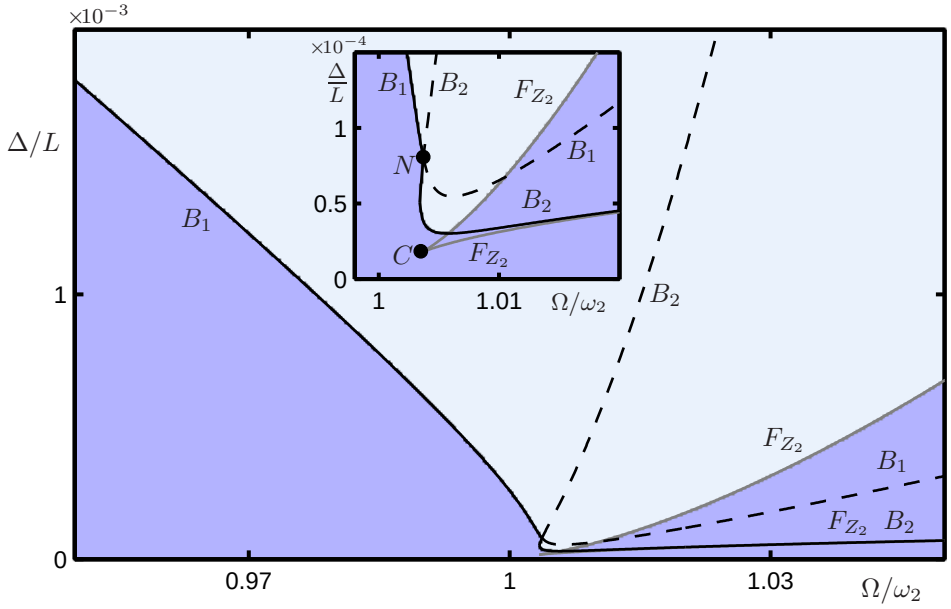

Fig. 4. Bifurcation diagram in the $(\Omega/\omega_2, \Delta/L)$-plane of the pure Z_2-response of (4), showing the bifurcation curves B_1 and B_2 and F_{Z_2} from Figs. 2(a) and 3(a). Along solid parts of the curves the bifurcation concerns a stable solution and along dashed parts it concerns an unstable one; the region where the pure Z_2-response is stable is shaded dark blue. The inset shows an enlargement near $\Omega/\omega_2 = 1$.

3.2. *The surface $\mathcal{L}_1$ of the coupled (Z_2, Y_1)-response*

The coupled (Z_2, Y_1)-response bifurcates from the pure Z_2-response along the branching bifurcation curve B_1. Figure 5(a) shows the associated surface $\mathcal{L}_1$ (green) of the coupled (Z_2, Y_1)-response in $(\Omega/\omega_2, \Delta/L, ||N||)$-space, which connects to the surface $\mathcal{L}$ (blue) along the curve B_1. Mathematically, this and all the other branching bifurcations we encounter are actually pitchfork bifurcations of (4): the two bifurcating equilibria differ only in the phase relationship between the contributing basic modes, which physically corresponds to clockwise or counter-clockwise whirling motion of the cable. Since the coupled modes are represented in terms of their norm $||N||$, these are not distinguished, and this is why one refers to this bifurcation as a branching bifurcation. The stable part of $\mathcal{L}_1$ (dark green) is bounded by the curve B_1 on $\mathcal{L}$ and by the branching bifurcation curve B^1_{12} on $\mathcal{L}_1$. As we will see in Sec. 3.4, the surface $\mathcal{L}_{12}$ of the coupled (Z_2, Y_1, Y_2)-response connects along B^1_{12}. Notice also the fold along F_{Y_1}. Highlighted in Fig. 5(a) are the cross sections of $\mathcal{L}$ and $\mathcal{L}_1$ for $\Omega/\omega_2 = 0.97$ and $\Omega/\omega_2 = 1.03$. Figure 5(b) shows the corresponding bifurcation diagram for $\Omega/\omega_2 = 0.97$ in the $(\Delta/L, ||N||)$-plane, which shows that a stable branch of the coupled (Z_2, Y_1)-response bifurcates from the pure Z_2-response at the branching bifurcation point B_1; compare with Fig. 3(b). The corresponding bifurcation diagram for $\Omega/\omega_2 = 1.03$ in the $(\Delta/L, ||N||)$-plane is shown in Fig. 5(c). An unstable branch of coupled (Z_2, Y_1)-response bifurcates from the point B_1, where the pure Z_2-response itself is also unstable. The branch of the coupled (Z_2, Y_1)-response remains unstable after the fold point F_{Y_1} but becomes stable after the branching bifurcation point B^1_{12}. Overall, Fig. 5 shows that, for any value of Ω/ω_2 the coupled (Z_2, Y_1)-response may be observed as a stable response provided that the excitation amplitude Δ/L is sufficiently large.

As it turns out, there is an additional part of the surface $\mathcal{L}_1$ that can be found when one considers it over a larger range of Ω/ω_2-values. Figure 6(a) shows the two surfaces $\mathcal{L}_1$ and $\mathcal{L}$ for $\Omega/\omega_2 \in [1.0, 1.07]$. Because of its complicated shape, the new part of the surface $\mathcal{L}_1$ is not rendered as a surface but represented by equally spaced (green) intersection curves for fixed Ω/ω_2. These intersection curves are connected for fixed $\Omega/\omega_2 > 1.05$ to the main part of the surface $\mathcal{L}_1$ along the fold curve F'_{Y_1}, which connects to the fold curve F_{Y_1} at $\Omega/\omega_2 \approx 1.05$. However, for fixed $\Omega/\omega_2 < 1.05$ we find figure-of-eight shaped isolas. Panels (b) and (c) of Fig. 6 show the two slices for $\Omega/\omega_2 = 1.03$ and for $\Omega/\omega_2 = 1.06$, respectively, which are also highlighted in panel (a). Notice the new isola of the coupled (Z_2, Y_1)-response for $\Omega/\omega_2 = 1.03$ in Fig. 6(b)

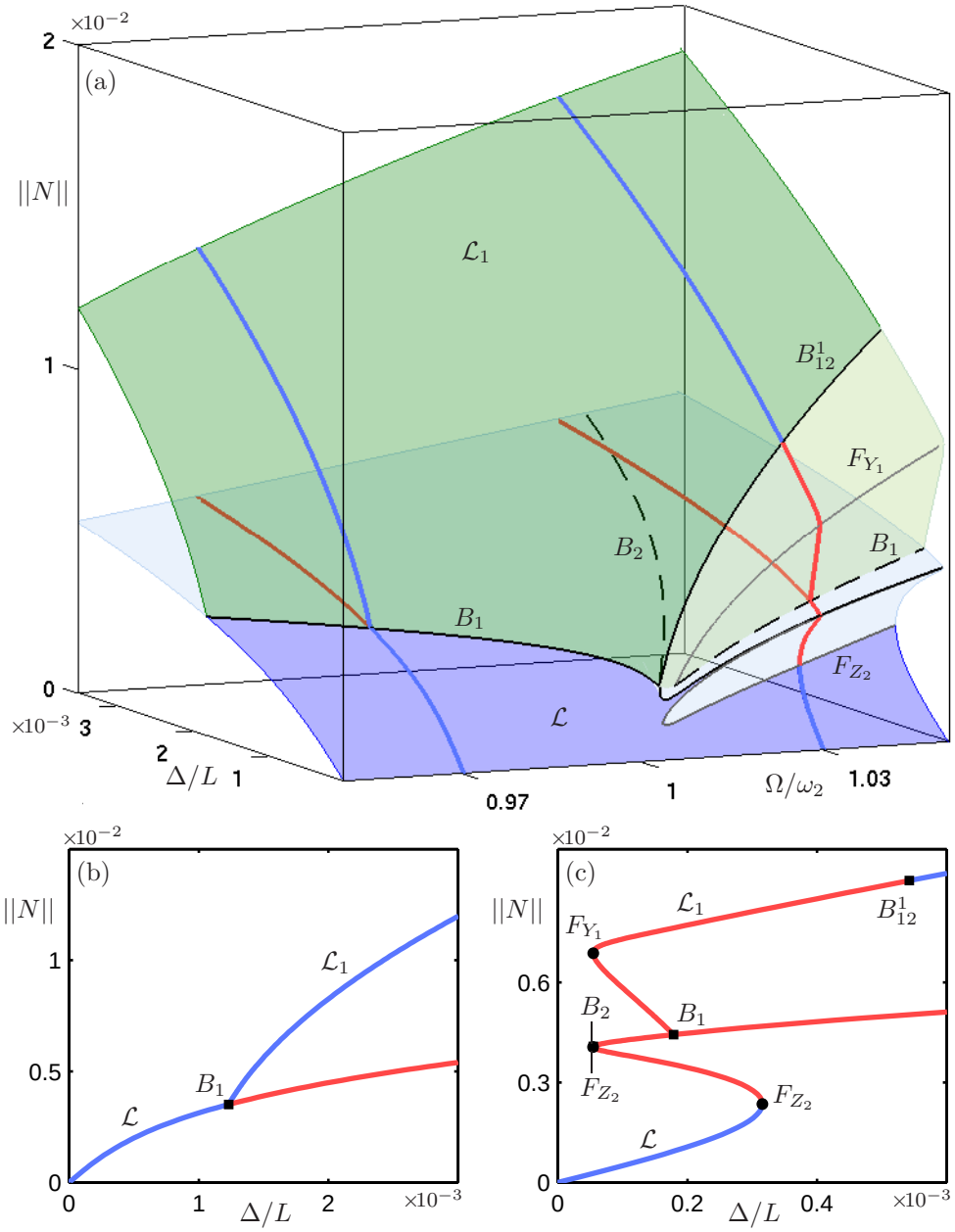

Fig. 5. Panel (a) shows the surface $\mathcal{L}_1$ (green) of the coupled (Z_2, Y_1)-response of (4) in $(\Omega/\omega_2, \Delta/L, ||N||)$-space, and how it connects to the surface $\mathcal{L}$ (blue) from Fig. 3. Also shown on $\mathcal{L}_1$ are the bifurcation curves B_{12}^1 and F_{Y_1}; the coupled (Z_2, Y_1)-response is stable in dark green part and unstable in light green part. Panels (b) and (c) show the one-parameter bifurcation diagrams in the $(\Delta/L, ||N||)$-plane for $\Omega/\omega_2 = 0.97$ and for $\Omega/\omega_2 = 1.03$, respectively; the corresponding curves are highlighted on the surfaces $\mathcal{L}_1$ and $\mathcal{L}$ in panel (a).

compared with Fig. 5(c). In the section for $\Omega/\omega_2 = 1.06$, on the other hand, we find a single connected curve of the coupled (Z_2, Y_1)-response. In both cases, there is a small region of stable (Z_2, Y_1)-response on the new curve.

Since these features of the surface $\mathcal{L}_1$ are hard to see on the scale of Fig. 6, we now focus on how the isola in the $(\Delta/L, ||N||)$-plane connects to the remainder of $\mathcal{L}_1$ as Ω/ω_2 is increased through 1.05. Figure 7 shows the intersection curves of $\mathcal{L}_1$ with cross sections for $\Omega/\omega_2 = 1.04$, for $\Omega/\omega_2 = 1.05$ and for $\Omega/\omega_2 = 1.06$ in the relevant part of the $(\Delta/L, ||N||)$-plane. Notice the figure-eight shape of the isola for $\Omega/\omega_2 = 1.04$ in Fig. 7(a); it is not actually connected at the two intersection point with the other

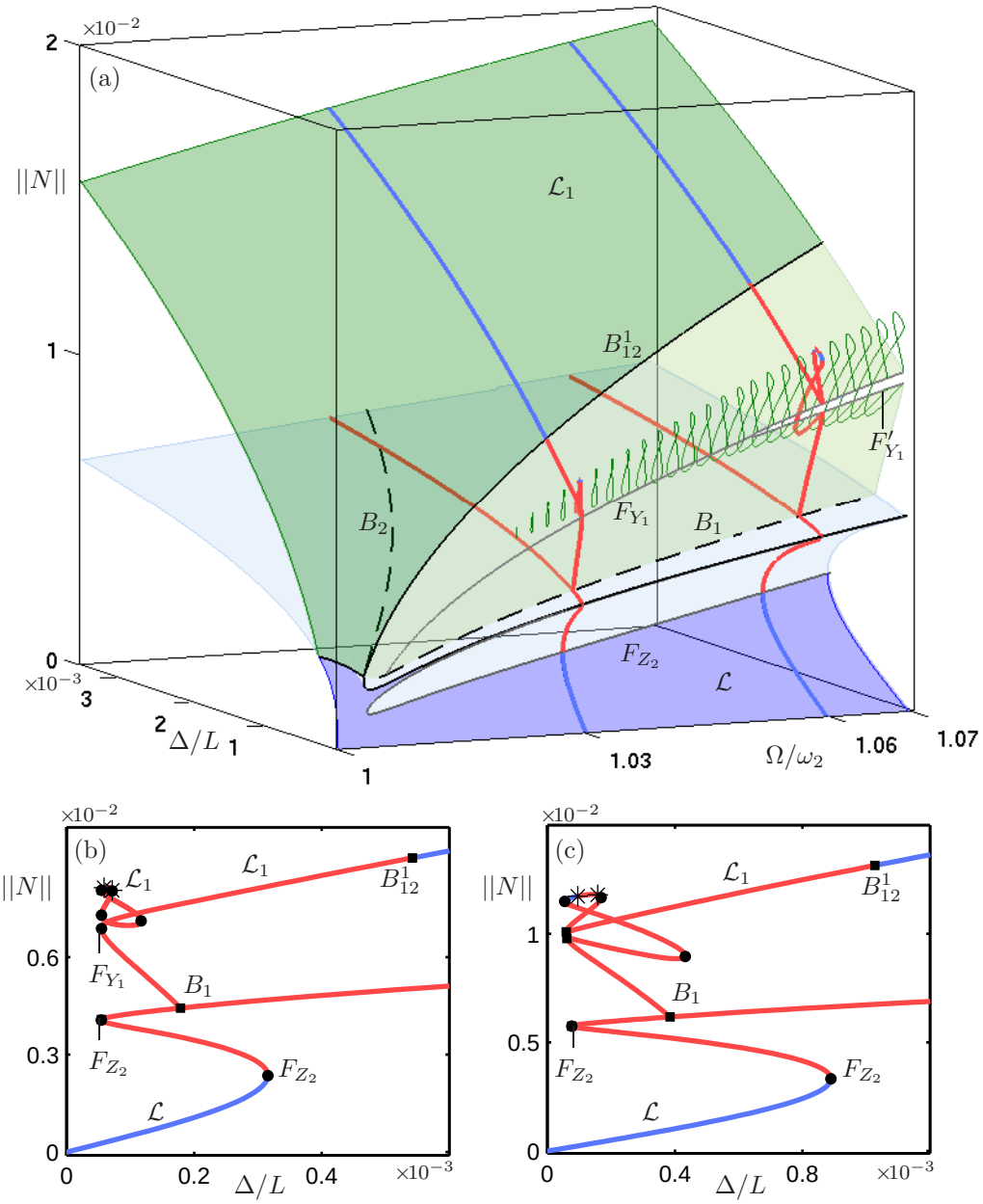

Fig. 6. Panel (a) shows the surfaces $\mathcal{L}_1$ (green) and $\mathcal{L}$ (blue) in $(\Omega/\omega_2, \Delta/L, ||N||)$-space over the range $\Omega/\omega_2 \in [1.0, 1.07]$. The new feature is an additional part of the surface $\mathcal{L}_1$ that is connected to its main part for $\Omega/\omega_2 > 1.05$ along the fold curve F'_{Y_1}, but also extends to smaller values of Ω/ω_2; due to its complicated shape, this new part of $\mathcal{L}_1$ is represented by intersections curves for fixed Ω/ω_2. The respective intersections for $\Omega/\omega_2 = 1.03$ and for $\Omega/\omega_2 = 1.06$ are highlighted. The corresponding bifurcation diagrams in the $(\Delta/L, ||N||)$-plane are shown in panels (b) and (c); there are two points of Hopf bifurcation (indicated by asterisks) on the additional branches of the coupled (Z_2, Y_1)-response.

intersection curve of $\mathcal{L}_1$. There are four fold points on the isola, which are labelled F_{Y_1} and F''_{Y_1}. At the moment of transition at $\Omega/\omega_2 \approx 1.05$ the lower fold point F_{Y_1} on the isola coincides with the fold point F_{Y_1} on the other branch; see Fig. 7(b). For $\Omega/\omega_2 = 1.06$ as in Fig. 7(c), there is now a single connected intersection curve of $\mathcal{L}_1$; the degenerate fold point has split up into two fold points labelled F'_{Y_1}. Notice that close to these fold points there are two branching bifurcation points that are labelled B_{12}^1; as we will see in Sec. 3.4, they lead to the bifurcating coupled (Z_2, Y_1, Y_2)-response.

Overall, Fig. 7 shows that the connectivity of the local branches near the point of transition changes.

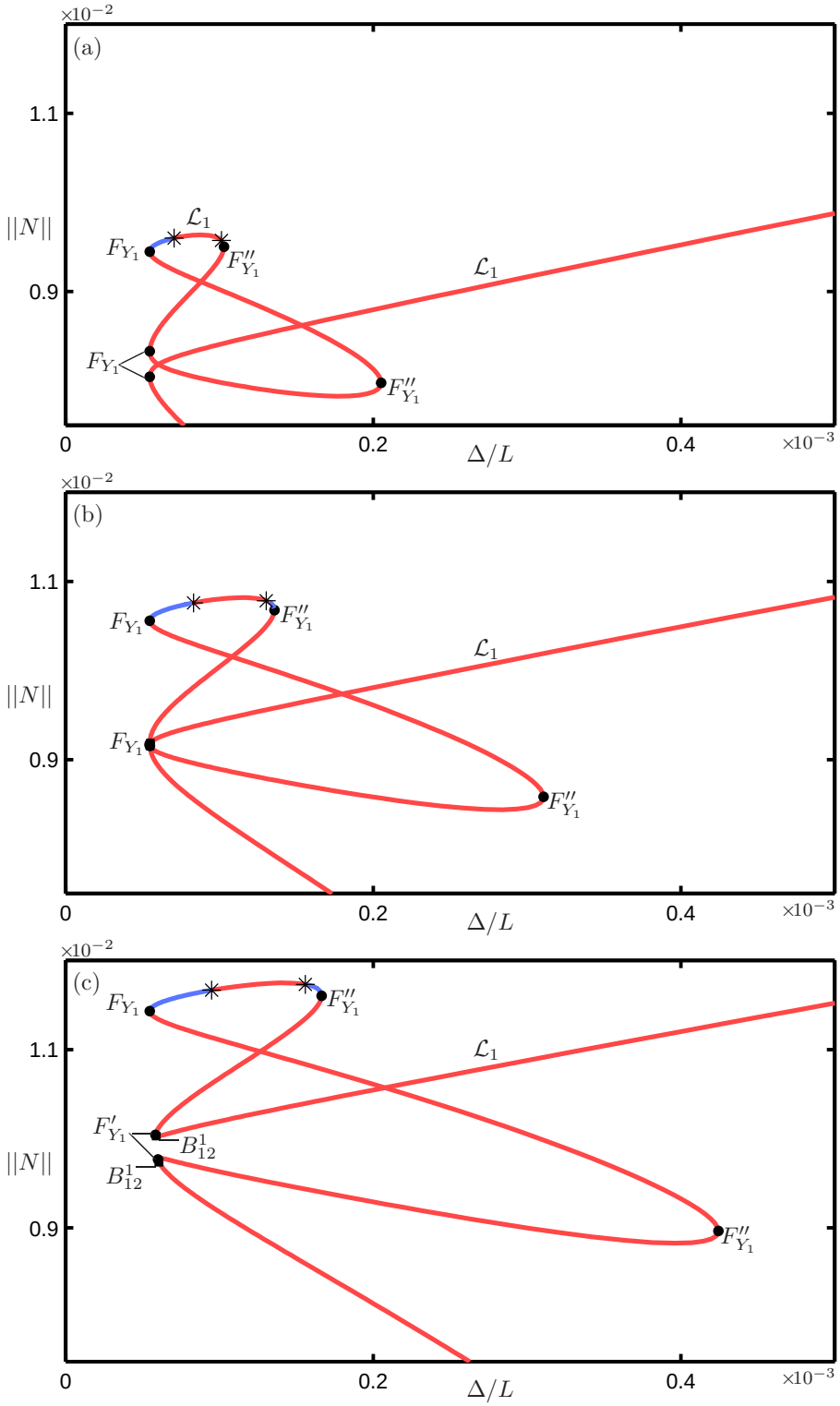

Fig. 7. One-parameter bifurcation diagrams of the coupled (Z_2, Y_1)-response in the $(\Delta/L, ||N||)$-plane for $\Omega/\omega_2 = 1.04$ in panel (a), for $\Omega/\omega_2 = 1.05$ in panel (b), and for $\Omega/\omega_2 = 1.06$ in panel (c). The ranges of Δ/L and $||N||$ are chosen to show how the isola of the coupled (Z_2, Y_1)-response for $\Omega/\omega_2 < 1.05$ connects to the remainder of the surface $\mathcal{L}_1$ when Ω/ω_2 is increased through $\Omega/\omega_2 \approx 1.05$; compare with Fig. 6.

This corresponds to a transition of the cross section through a critical point on the surface $\mathcal{L}_1$ in

$(\Omega/\omega_2, \Delta/L, ||N||)$-space. At this point the curve F_{Y_1} on $\mathcal{L}_1$ has a local maximum and the curve F'_{Y_1} on $\mathcal{L}_1$ has a local minimum with respect to Ω/ω_2; moreover, these two curves intersect transversally. The curve F'_{Y_1} and its minimum can be seen in Fig. 6(a). The curve F_{Y_1} is shown only up to the maximum where it meets F'_{Y_1}; its other part lies on the isola (green loops) and it is not shown in Fig. 6(a). Note that the curve of branching bifurcations B^1_{12} also passes through the critical point on $\mathcal{L}_1$ and has a minimum there with respect to Ω/ω_2. The isola can be found in the cross section for fixed Ω/ω_2 in the range $\Omega/\omega_2 \in (1.02, 1.05)$; see Fig. 6(a). It disappears at $\Omega/\omega_2 \approx 1.02$ by shrinking down to a point, which corresponds to a minimum with respect to Ω/ω_2 of the curve F_{Y_1} in $(\Omega/\omega_2, \Delta/L, ||N||)$-space.

In all three panels of Fig. 7 we also find a pair of Hopf bifurcations (denoted by asterisks). Moreover, the coupled (Z_2, Y_1)-response on the new part of $\mathcal{L}_1$ is stable between the (upper) fold point F_{Y_1} and the left-most point of Hopf bifurcation. Hence, we have found a new stable and, hence, observable (Z_2, Y_1)-response of the cable in the region of interest $\Omega/\omega_2 \in [0.95, 1.04]$, which is not connected to the main part of the surface $\mathcal{L}_1$ in this range of Ω/ω_2. This discovery justifies the consideration of the extended range of Ω/ω_2.

3.3. *The surface $\mathcal{L}_2$ of the coupled (Z_2, Y_2)-response*

Figure 8(a) shows the surface $\mathcal{L}_2$ of the coupled (Z_2, Y_2)-response, which is attached to the surface $\mathcal{L}$ along the branching bifurcation curve B_2. Almost all of $\mathcal{L}_2$ is unstable (light purple), but there is a small stable region (dark purple) near $\Omega/\omega_2 = 1$. On $\mathcal{L}_2$ there is a curve F_{Y_2} of fold bifurcation, whose left-most point is a cusp point. Moreover, we find a curve B^2_{12} of branching bifurcation that emerges from the point N where B_1 and B_2 intersect on $\mathcal{L}$; see Fig. 2. As with previous plots, two intersection sets are highlighted, namely those for $\Omega/\omega_2 = 1.007$ and $\Omega/\omega_2 = 1.03$, respectively; they are shown in the $(\Delta/L, ||N||)$-plane in Fig. 8(b) and (c).

The section for $\Omega/\omega_2 = 1.007$ in Fig. 8(b) passes through the stable part of $\mathcal{L}_2$. The branch $\mathcal{L}_2$ of the coupled (Z_2, Y_2)-response connects to the branch $\mathcal{L}$ of the pure Z_2-response at the two branching bifurcation points labelled B_2. The coupled (Z_2, Y_2)-response is stable right after the left-most branching bifurcation point B_2 on $\mathcal{L}$, and it loses its stability at the branching bifurcation point B^2_{12}; as we will see in Sec. 3.4, the coupled (Z_2, Y_1, Y_2)-response can be observed stably past this point. Notice from Fig. 8(b) that, as the excitation amplitude Δ/L is increased from zero, one first observes the pure Z_2-response until the fold point F_{Z_2} is reached, where the system transitions to a stable (Z_2, Y_2)-response.

The section for $\Omega/\omega_2 = 1.03$ in Fig. 8(c), on the other hand, misses the stable part on $\mathcal{L}_2$. Consequently, the branch $\mathcal{L}_2$ bifurcating from B_2 is unstable throughout, until it also reconnects with the branch of the pure Z_2-response at a second branching bifurcation point B_2 (which is outside the Δ/L-range shown in Fig. 8(c)). Notice the S-shaped nature of the branch $\mathcal{L}_2$ with two fold curves labelled F_{Y_2}.

3.4. *The surface $\mathcal{L}_{12}$ of the coupled (Z_2, Y_1, Y_2)-response*

The surface $\mathcal{L}_{12}$ of the coupled (Z_2, Y_1, Y_2)-response is quite complicated because it connects the two surfaces $\mathcal{L}_1$ of the coupled (Z_2, Y_1)-response and $\mathcal{L}_2$ of the coupled (Z_2, Y_2)-response. In Fig. 9(a), it is shown together with only the surface $\mathcal{L}_2$ from Fig. 8(a) to which it is attached along the curve B^2_{12}. The (dark brown) stable part of $\mathcal{L}_{12}$ in Fig. 9(a) is bounded at the top by the curve B^1_{12}, along which this surface is connected to the surface $\mathcal{L}_1$ of the coupled (Z_2, Y_1)-response (which is not shown); compare with Fig. 6(a). The lower boundary of the stable part of $\mathcal{L}_{12}$ is more complicated: at low values of Ω/ω_2 it is the same curve B^2_{12}, and for higher values of Ω/ω_2 it is formed by fold curve $F_{Y_{12}}$ on $\mathcal{L}_{12}$. Specifically, between $F_{Y_{12}}$ and B^2_{12} there are two other boundaries of $\mathcal{L}_{12}$, namely the fold curve $F^1_{Y_{12}}$ and the Hopf bifurcation curve H_{12}. In fact, $F^1_{Y_{12}}$ emerges from a point on B^2_{12} and H_{12} emerges from a point on B^2_{12}. This structure of the boundary of the coupled (Z_2, Y_1, Y_2)-response was also found in [Marsico *et al.*, 2011] for a four-mode model that includes the first in-plane mode.

Two of the three highlighted intersection sets in Fig. 9(a) are shown separately in the $(\Delta/L, ||N||)$-plane as panels (b) and (c); for clarity, the stable and unstable regions of $\mathcal{L}$ are also shown as black and grey curves, respectively. In Fig. 9(b) for $\Omega/\omega_2 = 1.007$, which builds on Fig. 8(b), the branch $\mathcal{L}_{12}$

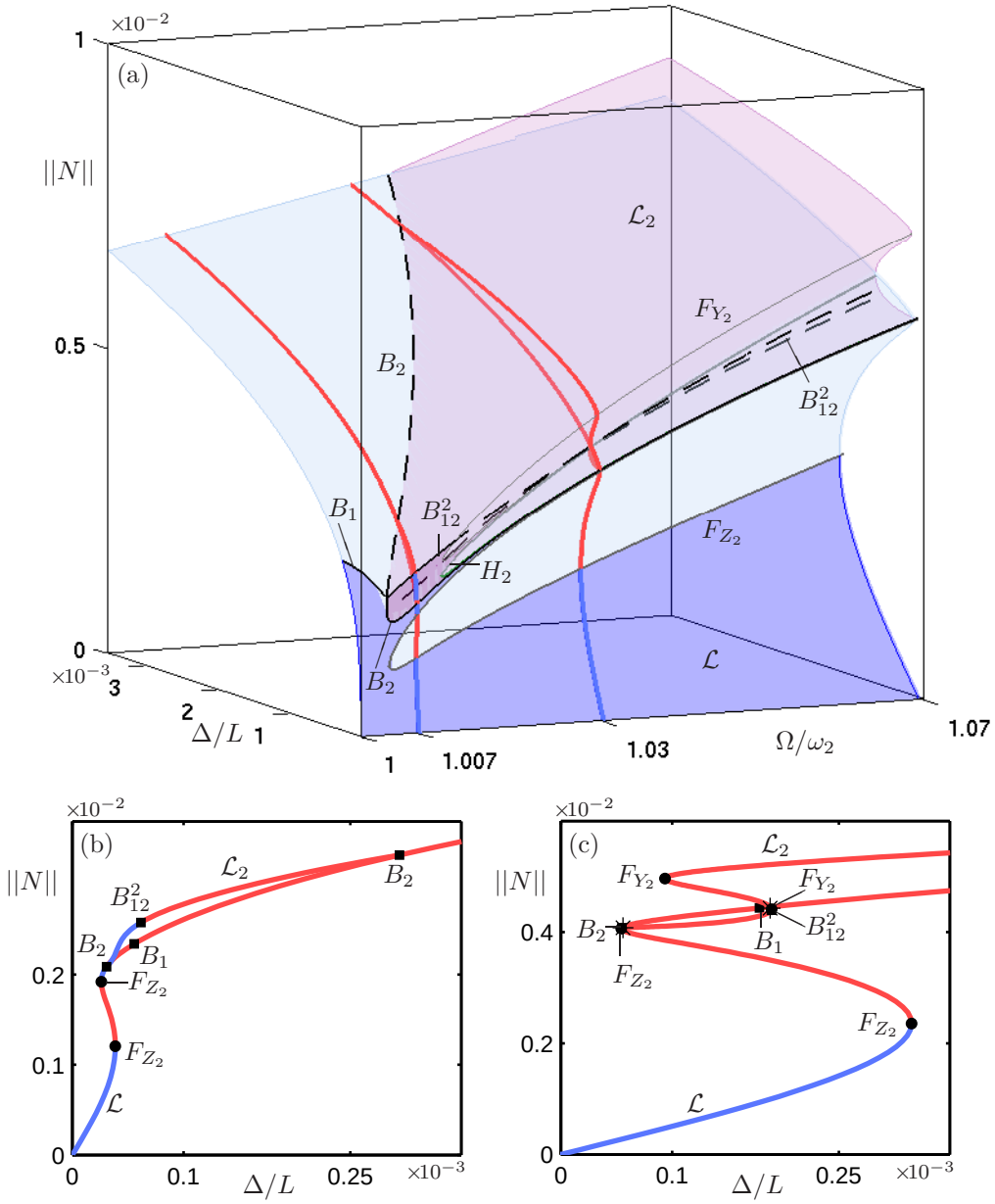

Fig. 8. Panel (a) shows the surface $\mathcal{L}_2$ (purple) of the coupled (Z_2, Y_2)-response of (4) in $(\Omega/\omega_2, \Delta/L, ||N||)$-space, and how it connects to the surface $\mathcal{L}$ (blue) from Fig. 3. Also shown on $\mathcal{L}_2$ are the bifurcation curves F_{Y_2} and B_{12}^2; the coupled (Z_2, Y_2)-response is stable in the small dark purple part only. Panels (b) and (c) show the one-parameter bifurcation diagrams in the $(\Delta/L, ||N||)$-plane for $\Omega/\omega_2 = 1.007$ and for $\Omega/\omega_2 = 1.03$, respectively; the corresponding curves are highlighted on the surfaces $\mathcal{L}_2$ and $\mathcal{L}$ in panel (a).

bifurcates from the point B_{12}^2 on the branch $\mathcal{L}_2$; along this branch the coupled (Z_2, Y_1, Y_2)-response is stable. Figure 9(c) for $\Omega/\omega_2 = 1.03$ builds on Fig. 8(c). Now the branch $\mathcal{L}_{12}$ has three fold points; it is stable only after the last fold point labelled $F_{Y_{12}}$. Notice that in between the upper fold point and a point H_{12} of Hopf bifurcation (denoted by an asterisk) there is an additional tiny part of the branch where the coupled (Z_2, Y_1, Y_2)-response is stable; this Hopf bifurcation curve is shown in Fig. 9(a). Finally, we remark that Fig. 9(c) shows that, as Δ/L is increased from zero, the transition to different dynamics when the pure Z_2-response loses stability at F_{Z_2} now results in a (Z_2, Y_1, Y_2)-response of the cable.

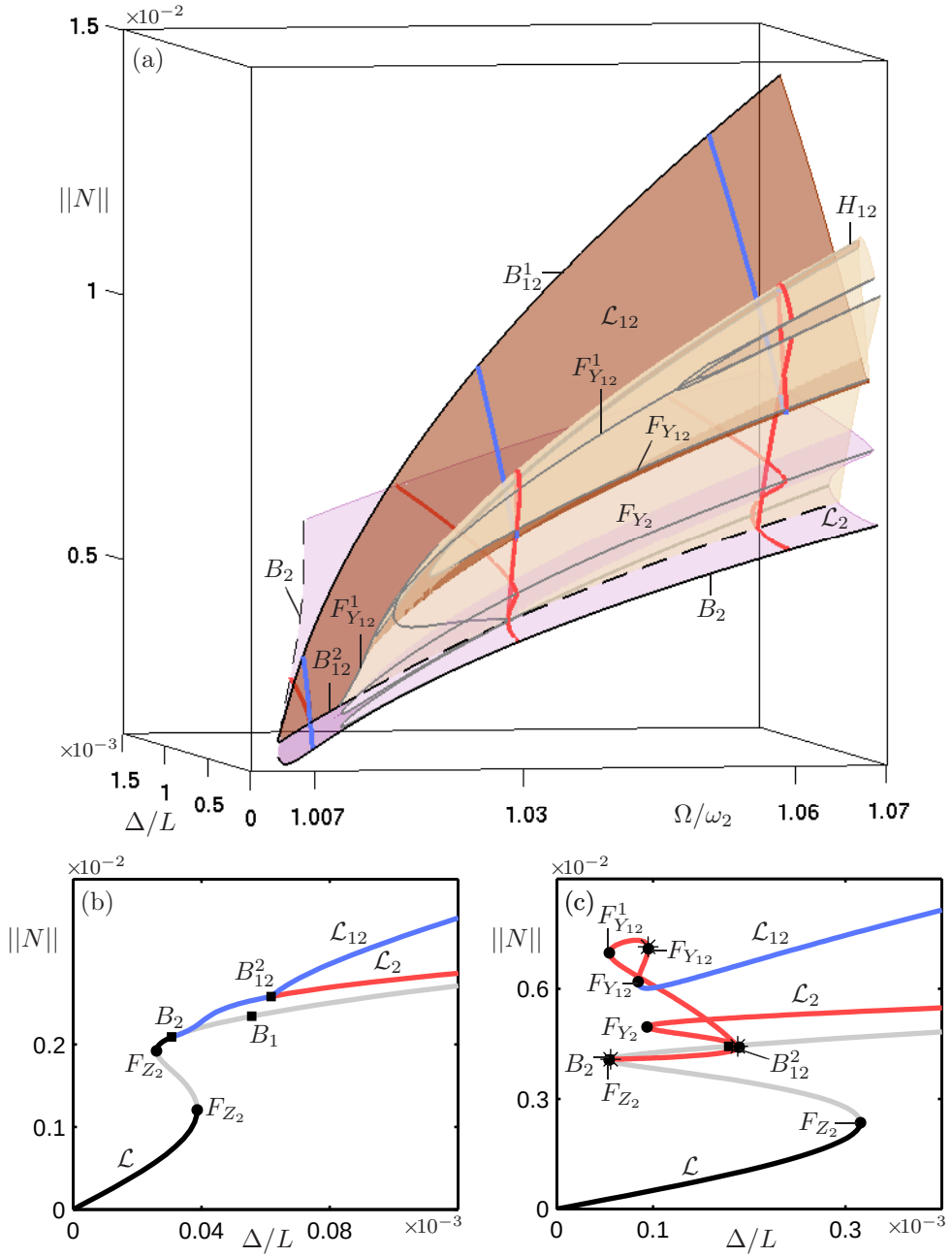

Fig. 9. Panel (a) shows the surface $\mathcal{L}_{12}$ (brown) of the coupled (Z_2, Y_1, Y_2)-response of (4) in $(\Omega/\omega_2, \Delta/L, ||N||)$-space, and how it connects to the surface $\mathcal{L}_2$ (purple) from Fig. 8. The coupled (Z_2, Y_1, Y_2)-response is stable in the dark brown part of $\mathcal{L}_{12}$ and unstable in the light brown part. The intersection sets for $\Omega/\omega_2 = 1.007$, for $\Omega/\omega_2 = 1.03$, and for $\Omega/\omega_2 = 1.06$ are highlighted; those for $\Omega/\omega_2 = 1.007$ and for $\Omega/\omega_2 = 1.03$ are shown in the $(\Delta/L, ||N||)$-plane in panels (b) and (c), respectively, and that for $\Omega/\omega_2 = 1.06$ appears as part of Fig. 11(c).

3.5. *Overall bifurcation structure with all four surfaces*

Figure 10 shows the surfaces $\mathcal{L}$ (blue), $\mathcal{L}_1$ (green), $\mathcal{L}_2$ (purple) and $\mathcal{L}_{12}$ (brown) together in $(\Omega/\omega_2, \Delta/L, ||N||)$-space. It constitutes a bifurcation diagram of the pure Z_2-response, the coupled (Z_2, Y_1)-response, the coupled (Z_2, Y_2)-response and the coupled (Z_2, Y_1, Y_2)-response, which represent all the equilibrium solutions of (4) and, hence, the responses of the cable with fixed amplitudes of the contributing three basic in-plane and out-of-plane modes. These different surfaces meet at curves of branch point bifurcations; specifically, $\mathcal{L}_1$ meets $\mathcal{L}$ along B_1 [see Sec. 3.2 and Fig. 6], $\mathcal{L}_2$ meets $\mathcal{L}$ along B_2 [see Sec. 3.3 and

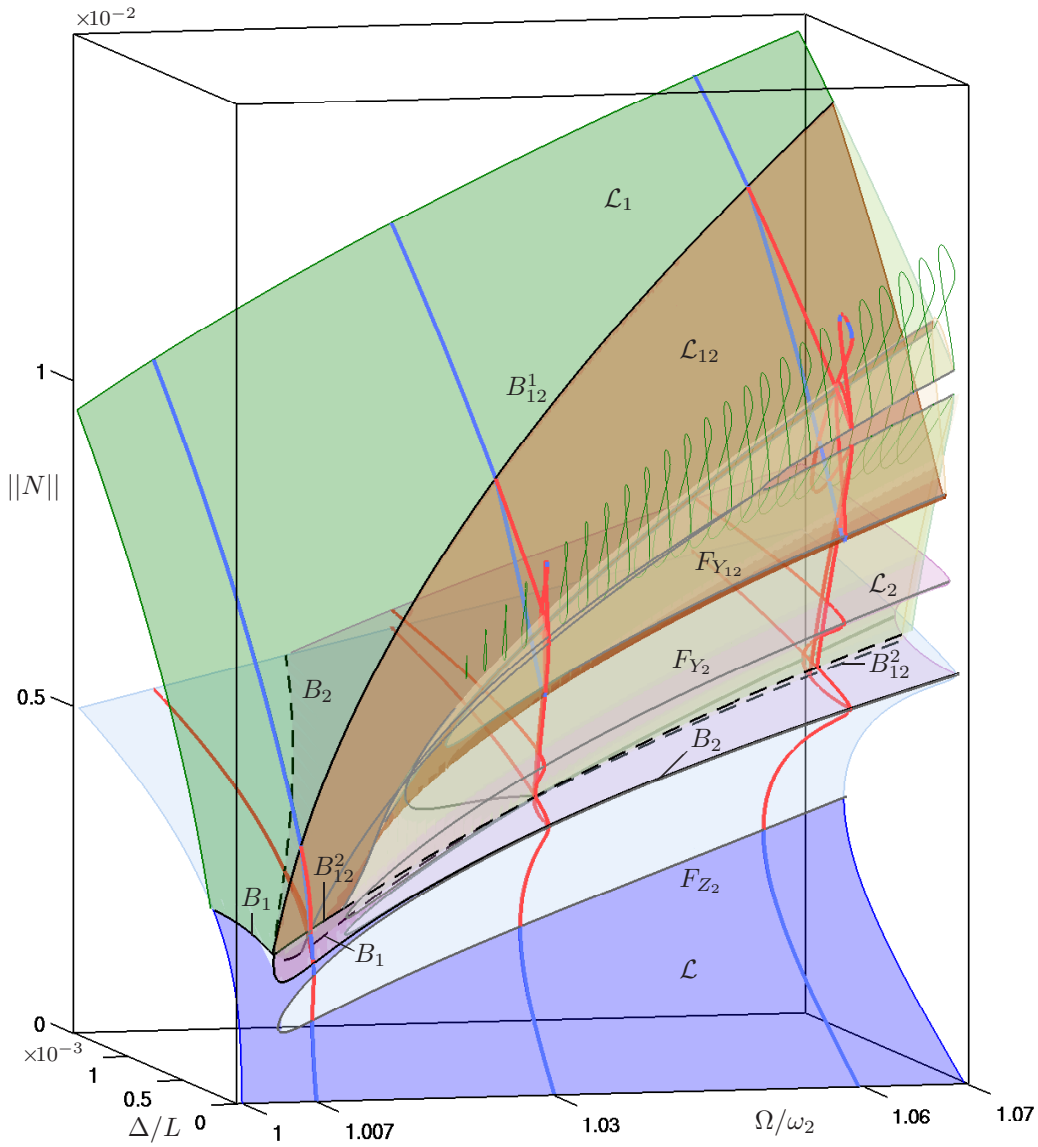

Fig. 10. The surfaces $\mathcal{L}$ (blue), $\mathcal{L}_1$ (green), $\mathcal{L}_2$ (purple) and $\mathcal{L}_{12}$ (brown) shown in $(\Omega/\omega_2, \Delta/L, ||N||)$-space together with the various curves of bifurcations on them. The intersection sets for $\Omega/\omega_2 = 1.007$, $\Omega/\omega_2 = 1.03$ and $\Omega/\omega_2 = 1.06$ are highlighted; darker colours represent stable modes. The intersection sets for $\Omega/\omega_2 = 1.007$, for $\Omega/\omega_2 = 1.03$ and for $\Omega/\omega_2 = 1.06$ are highlighted; they are shown in the $(\Delta/L, ||N||)$-plane in Fig. 11.

Fig. 8], and $\mathcal{L}_{12}$ meets $\mathcal{L}_1$ along B^1_{12} and $\mathcal{L}_2$ along B^2_{12} [see Sec. 3.4, and Fig. 9]. Stable parts of the surfaces are represented by darker colours and unstable parts by lighter colours; the respective curves of branching bifurcations are shown as solid curves where they connect two stable surfaces and as dashed curves where they connect two unstable surfaces. Also shown in Fig. 10 are the different curves of fold bifurcation.

The bifurcation diagram in Fig. 10 is shown for the range $\Omega/\omega_2 \in [1.0, 1.07]$ where the surfaces and corresponding modes interact strongly. Note that for $\Omega/\omega_2 \leq 1$, only the surfaces $\mathcal{L}$ and $\mathcal{L}_1$ meet along the curve B_1; see Figs. 5 and 6. This is visible already on the left-hand side of Fig. 10, so that this bifurcation diagram represents the topological nature of the equilibria of (4) and their stability over the range of $\Omega/\omega_2 \in [0.97, 1.0]$ that we consider here. As before, even though it may be at the limit of validity of the three-mode model (4) considered here, the range $\Omega/\omega_2 \in [1.04, 1.07]$ is specifically included due to the nature of the surface $\mathcal{L}_1$.

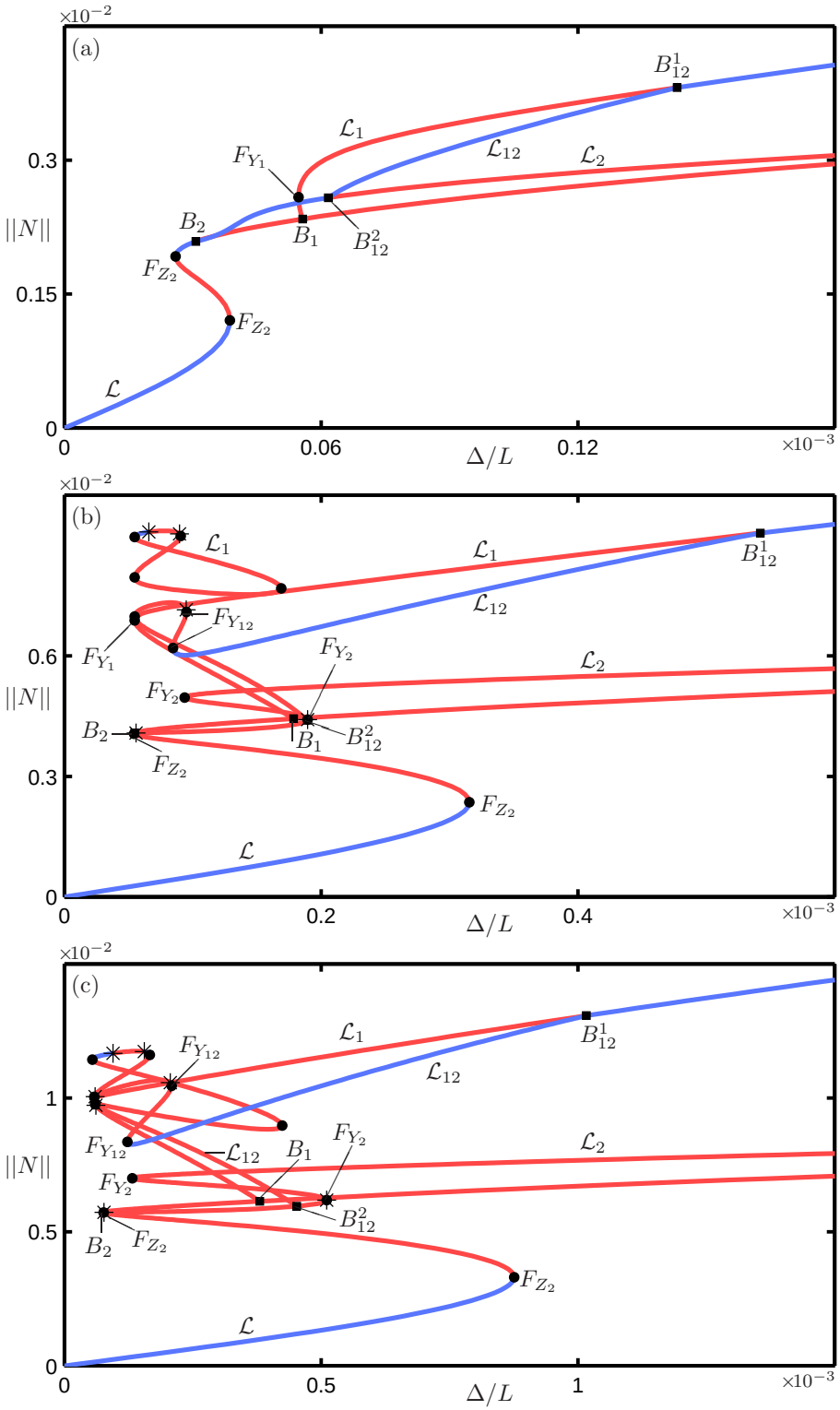

Fig. 11. One-parameter bifurcation diagrams of (4) in the $(\Delta/L, ||N||)$-plane for $\Omega/\omega_2 = 1.007$ in panel (a), for $\Omega/\omega_2 = 1.03$ in panel (b), and for $\Omega/\omega_2 = 1.06$ in panel (c); compare with Fig. 10. Blue curves denote stable and red curves denote unstable constant-amplitude solutions; branching bifurcation points are denoted by squares, fold points by dots, and Hopf bifurcation points by asterisks.

The three intersection sets for $\Omega/\omega_2 = 1.007$, $\Omega/\omega_2 = 1.03$ and $\Omega/\omega_2 = 1.06$ are highlighted on the surfaces in Fig. 10. They are shown as one-parameter bifurcation diagrams for all of the modes in the $(\Delta/L, ||N||)$-plane in Fig. 11(a)–(c).

For fixed $\Omega/\omega_2 = 1.007$, as is shown in Fig. 11(a), as Δ/L is increased from zero, the cable first experiences vibrations in the pure Z_2-response. At F_{Z_2} a transition occurs to the stable part of the branch $\mathcal{L}_2$ of the coupled (Z_2, Y_2)-response, meaning that now the second out-of-plane mode also contributes to the cable response. When Δ/L is increased further, past B^2_{12}, one observes also the gradual onset of the first out-of-plane mode to the cable response when B^2_{12} is crossed to the stable part of the branch $\mathcal{L}_{12}$. For even higher Δ/L the contribution from Y_2 disappears gradually at B^1_{12}, and one is left with the coupled (Z_2, Y_1)-response along the stable part of $\mathcal{L}_1$. When Δ/L is decreased again, one observes a gradual transition from the coupled (Z_2, Y_1)-response via the coupled (Z_2, Y_1, Y_2)-response and the coupled (Z_2, Y_2)-response to the pure Z_2-response. However, there is then a transition at F_{Z_2} to the lower branch of $\mathcal{L}$, that is, to a pure Z_2-response with lower amplitude, which is part of a small hysteresis loop.

For fixed $\Omega/\omega_2 = 1.03$, as is shown in Fig. 11(b), the bifurcation diagram in the $(\Delta/L, ||N||)$-plane is considerably more complicated. The transition from the stable pure Z_2-response at F_{Z_2} now results in a coupled (Z_2, Y_1, Y_2)-response of the cable along the stable part of $\mathcal{L}_{12}$. When Δ/L is increased the Y_2-contribution gradually disappears at B^1_{12}, and one is again left with the coupled (Z_2, Y_1)-response along the stable part of $\mathcal{L}_1$. When Δ/L is decreased, starting from the stable part of $\mathcal{L}_{12}$, the coupled (Z_2, Y_1, Y_2)-response is observed until the fold point $F_{Y_{12}}$ is reached. Then the system makes a transition to a different response. It is actually not entirely clear from the bifurcation diagram in Fig. 11(b) to which response the system will move at this point. After all, there is now a considerable amount of multi-stability between different modes. Moreover, there are points of Hopf bifurcation (denoted by asterisks) that give rise to periodic solutions, some of which are stable, for example, past the left-most Hopf bifurcation on the isola of $\mathcal{L}_1$. There is also the possibility that such periodic orbits bifurcate further to more complicated stable dynamics of the cable. This motivates the study of periodic solutions and their bifurcations in Sec. 4.

Finally, for $\Omega/\omega_2 = 1.06$, as is shown in Fig. 11(c), the one-parameter bifurcation diagram is very much as that for $\Omega/\omega_2 = 1.03$ in Fig. 11(b). As was discussed in Sec. 3.2, the difference is that $\mathcal{L}_1$ is a single branch that now incorporates the former isola. However, in terms of observed stable behaviour of the cable, the two cases are effectively the same.

3.6. *Bifurcation diagram and hysteresis loops*

From a practical point of view, it is useful to be able to identify for which combination of excitation frequency and amplitude the different types of coupled mode response of the cable can be found. Therefore, we present in Fig. 12 a bifurcation diagram in the $(\Omega/\omega_2, \Delta/L)$-plane with the regions where the different constant-amplitude responses are stable. Figure 12(a) is a projection of the stable parts of the surfaces $\mathcal{L}_1$ (green), $\mathcal{L}_2$ (purple) and $\mathcal{L}_{12}$ (brown) onto the relevant part of the $(\Omega/\omega_2, \Delta/L)$-plane, and Fig. 12(b) shows the stability region (blue) of the pure Z_2-response over the same parameter range; compare with Fig. 4. Note that the pure Z_2-response is stable throughout the white region in Fig. 12(a); moreover, to the right of the point N the stability regions in panels (a) and (b) of Fig. 12 overlap, yielding a considerable region of multistability between different constant-amplitude cable responses. Overall, Fig. 12 represents a practical bifurcation chart for the observable constant-amplitude dynamics of the cable. In Fig. 12(a) we show only the bifurcation curves that bound the respective stability regions. They include the curves H_2 on $\mathcal{L}_2$ and H_{12} on $\mathcal{L}_{12}$ of Hopf bifurcations, which bound the stability regions of $\mathcal{L}_2$ and $\mathcal{L}_{12}$, respectively. There are two additional codimension-two bifurcation points where different curves meet: the point M where B^2_{12} and $F^1_{Y_{12}}$ meet, and the point Q where $F^1_{Y_{12}}$ and H_{12} meet. Notice, in particular, the very thin strip of the (purple) stability region of $\mathcal{L}_2$ that is bounded by the curves B_2 and H_2. Similarly, there is an extremely thin strip of the stability region of $\mathcal{L}_{12}$ between the curves $F_{Y_{12}}$ and H_{12}, which correspond to a region of bi-stability of the coupled (Z_2, Y_1, Y_2)-response. We remark that these two thin strips of stability would be virtually impossible to find in an experiment. However, if another parameter, such as the damping ratio, is changed then these regions of bi-stability may be considerably larger [Tzanov *et al.*, 2011].

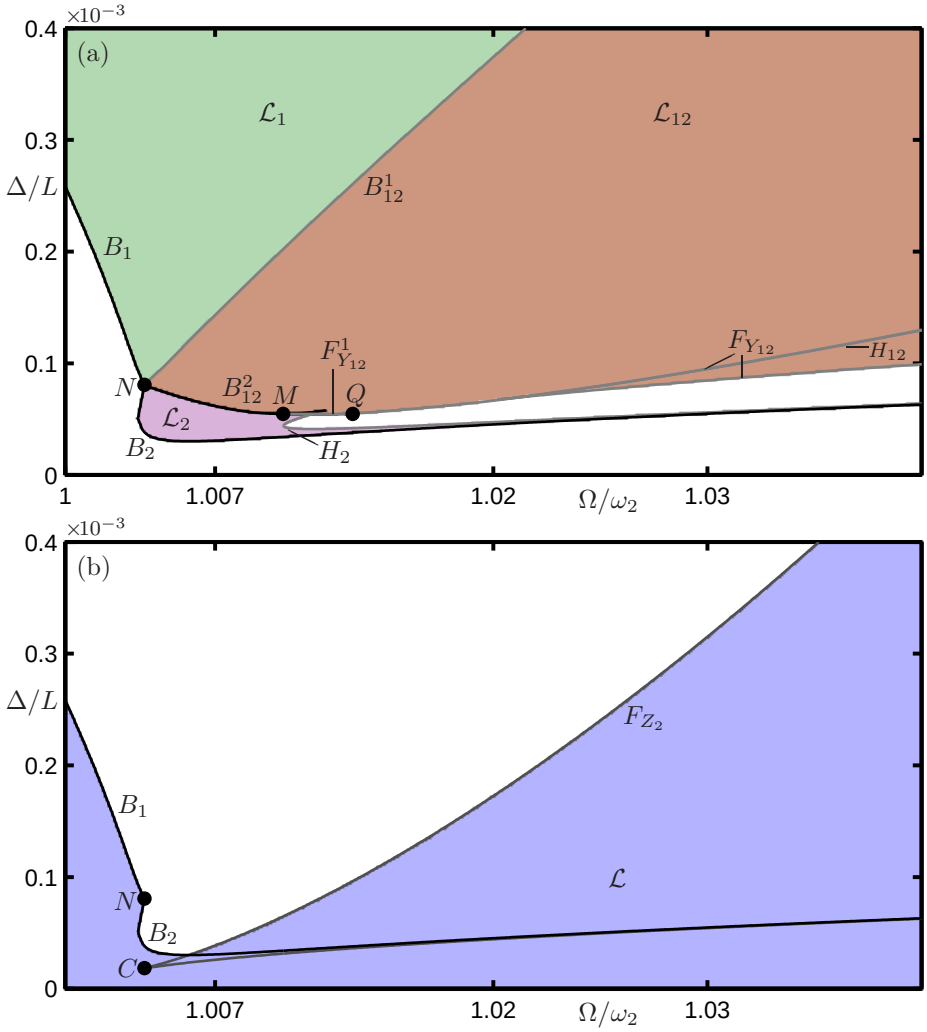

Fig. 12. Panel (a) shows the projection of the stable parts of the surfaces $\mathcal{L}_1$ (green), $\mathcal{L}_2$ (purple) and $\mathcal{L}_{12}$ (brown) onto the $(\Omega/\omega_2, \Delta/L)$-plane, where $\Omega/\omega_2 \in [1, 1.04]$ and $\Delta/L \in [0, 0.0075]$. Panel (b) shows the stable part of the surface $\mathcal{L}$ in the same region of the $(\Omega/\omega_2, \Delta/L)$-plane.

The bifurcation diagram in Fig. 12 represents a practical overview of the observable constant-amplitude dynamics of the cable, as represented by the equilibria of (4), and it is instructive to consider how they can be observed and distinguished in practice. A main measurement in experiments is to record the y- and z-components of the motion at the quarter points by means of video capture; this results in a quarter-span trace in the (y, z)-plane; see [Gonzalez-Buelga *et al.*, 2008; Marsico *et al.*, 2011]. The pure Z_2-response, which corresponds to a vertical standing wave, gives a quarter-span trace in the form of a vertical line. The coupled (Z_2, Y_1)-response, the coupled (Z_2, Y_2)-response and the coupled (Z_2, Y_1, Y_2)-response, on the other hand, correspond to whirling of the cable, and they lead to quarter-span traces in the form of closed curves. The respective traces can be found from numerical simulations of the full Warnichai equations (1), where the initial conditions are derived from the AUTO data generated in the bifurcation analysis of the averaged system (4); throughout, we use the Matlab routine ODE45 for simulations of (1). The output of the simulation is then plotted as $(y, z) = (y_1/\sqrt{2} + y_2, z_2)$; this is the quarter-span trace under the assumption that the mode-shapes are sinusoidal, which is accurate for taut cables [Wagg & Neild, 2010]. Figure 13 shows two examples, taken from stable branches of Fig. 14. Specifically, Fig. 13(a) is the quarter-span trace of the coupled (Z_2, Y_2)-response for $\Delta/L = 0.038 \times 10^{-3}$, which is on $\mathcal{L}_2$ between the points B_2 and H_2. This trace is a single close curve without self-intersections, owing to the fact that the

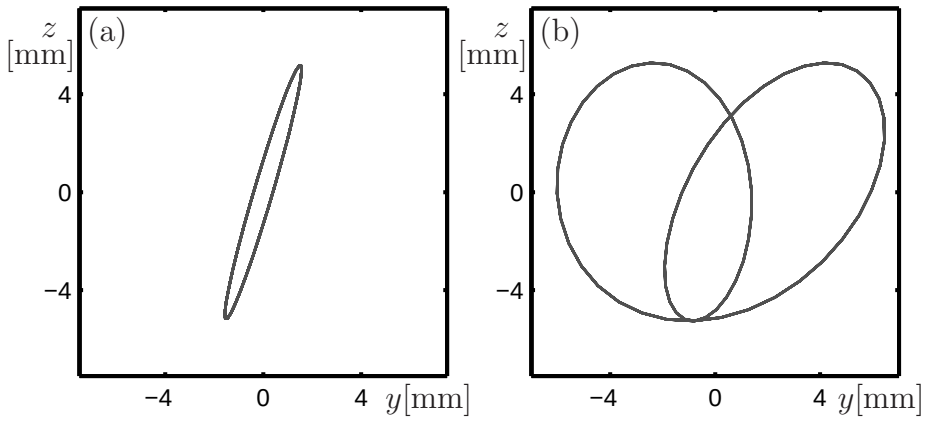

Fig. 13. Quarter-span trace of the coupled (Z_2, Y_2)-response for $\Omega/\omega_2 = 1.013$ and $\Delta/L = 0.038 \times 10^{-3}$ (a), and of the coupled (Z_2, Y_1, Y_2)-response for $\Omega/\omega_2 = 1.013$ and $\Delta/L = 0.086 \times 10^{-3}$ (b).

two basic modes involved are 1 : 1 locked. Figure 13(b) is the quarter-span trace of the coupled (Z_2, Y_1, Y_2)-response for $\Delta/L = 0.086 \times 10^{-3}$, which is on $\mathcal{L}_{12}$ to the right of the point H_{12}. The trace is again a single closed curve, but now with self-intersections due to 2 : 1 locking between the three basic modes involved. We remark that the quarter-span traces in Figure 13 are traversed counter-clockwise; there also exist the corresponding clockwise traces, which can be obtained from the shown ones by reflecting them in the y-axis.

In experiments, such as those in [Gonzalez-Buelga *et al.*, 2008; Marsico *et al.*, 2011], the forcing amplitude Δ/L is changed for a fixed given value of the forcing frequency Ω/ω_2. Owing to the considerable amount of multistability of the system, it is quite difficult to predict from Fig. 12 the exact sequence of cable responses that will be observed as Δ/L is increased and/or decreased. To understand this in detail, the one-paramter bifurcation diagram in Δ/L for the given fixed Ω/ω_2 needs to be considered. So far, we have presented one-paramter bifurcation diagrams as cross-section through the different surfaces of constant-amplitude responses to illustrate their exact relative positions. We now demonstrate that additional important information on the observed cable dynamics can be obtained from a one-paramter bifurcation diagram.

Figure 14 shows the one-parameter bifurcation diagram in the $(\Delta/L, ||N||)$-plane of the equilibria of (4) for $\Omega/\omega_2 = 1.013$. Note that this value of the forcing frequency is quite close to the ω_2, yielding a bifurcation diagram that is moderately complicated, in between those shown in Fig. 11(a) and (b). Nevertheless, as the enlargement in Fig. 14(b) illustrates, there is already a considerable amount of multistability between the different modes. Moreover, each of the stable parts of branches is bounded by a fold curve (except that $\mathcal{L}_{12}$ is bounded by H_{12}, which lies indistinguishably close to F^1_{12}). Changing Δ/L past such a fold curve leads to a loss of the attractor and the system transitions to a different attractor. These transitions are illustrated in Fig. 14 with arrows J_1, J_2, J_3 and J_4 denoting to transitions from $\mathcal{L}$, $\mathcal{L}_{12}$ and $\mathcal{L}_2$, and from a higher amplitude on $\mathcal{L}_2$, respectively. These transitions define two hysteresis loops as Δ/L is swept up and down: the first consists of transitions J_1, J_2 and J_3, and the second is formed by J_2 and J_4.

Even in the presence of small perturbations on the level of the measurement uncertainty of an experiment, the transition J_1 always ends on the only available stable part of the branch $\mathcal{L}_{12}$, so that it is a transition from the pure Z_2-response to the coupled (Z_2, Y_1, Y_2)-response; hence, this transition corresponds to the quite sudden onset of large-amplitude whirling motion of the cable. Similarly, transition J_3 always ends on the stable part of $\mathcal{L}$, corresponding to a disappearance of whirling and the transition to large-amplitude vertical cable response. Transition J_4 is different in this respect. It can end up on the stable part of the branch $\mathcal{L}_{12}$, as is indicated by the arrow in Fig. 14(b). However, depending on the kind of perturbation just past the fold point F_{Y_2}, it may also end up at a different dynamic state that does not have constant amplitudes of the participating basic modes. Finally, transition J_2 does never end up at constant-amplitude cable motion, because none of the four constant-amplitude responses is stable in

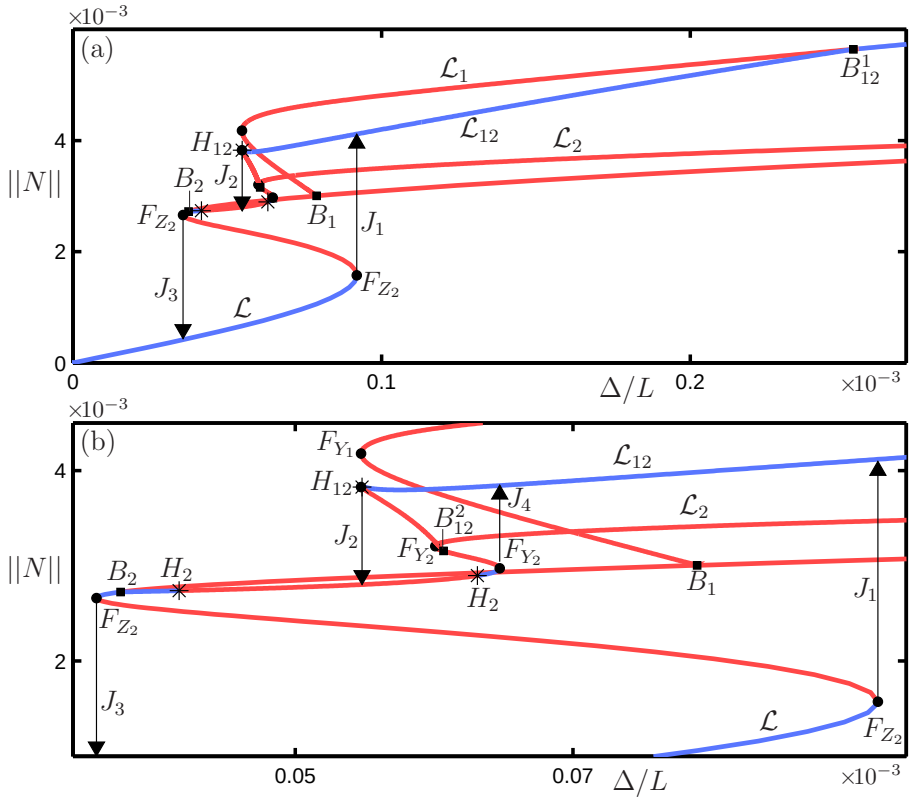

Fig. 14. Panel (a) shows the one-parameter bifurcation diagram of (4) in the $(\Delta/L, ||N||)$-plane for $\Omega/\omega_2 = 1.013$. Blue curves denote stable and red curves denote unstable equilibria; branching bifurcation points are denoted by squares, fold points by dots, and Hopf bifurcation points by asterisks. Also shown are four transitions J_1, J_2, J_3 and J_4 from stable equilibria that occur when Δ/L is increase or decreased past fold points. Panel (b) is an enlargement that focuses on range where these transitions occur.

this range of Δ/L; see Fig. 14(b). Rather, J_2 always results in cable dynamics with varying amplitudes of the basic modes. The nature of these transitions was determined by numerical simulations of the full Warnichai equations (1) subject to parameter drift in Δ/L in the presence of suitable perturbations; see [Tzanov, 2012] for details.

4. Cable Response with Varying Amplitudes

We now focus on cable dynamics in the intermediate range of Δ/L near transition J_2. As it turns out, the cable dynamics in this range takes place near the branch $\mathcal{L}_2$ of the coupled (Z_2, Y_2)-response; it is stable, on the left between the points B_2 and H_2, and on the right between the bifurcation points H_2 and F_{Y_2}; see in Fig. 14(b). However, in the Δ/L-range of interest the coupled (Z_2, Y_2)-response is unstable. The existence of the two Hopf bifurcations that form the stability boundary of $\mathcal{L}_2$ implies that there are bifurcating periodic orbits of (4). In fact, they all have contributions from the second in-plane mode and the second out-of-plane mode only, and not from the first out-of-plane mode (that is, $Y_1 = 0$ throughout). Moreover, they undergo the following bifurcations:

$F_1^{H_2}$ and $F_2^{H_2}$ denote fold (saddle-node) bifurcations of periodic orbits;

PD_1 and PD_2 denote period-doubling bifurcations of a basic periodic orbit;

PD_1^2 and PD_2^2 denote period-doubling bifurcations of a period-doubled periodic orbit;

$\mathscr{S}$ denotes a Shilnikov homoclinic bifurcation.

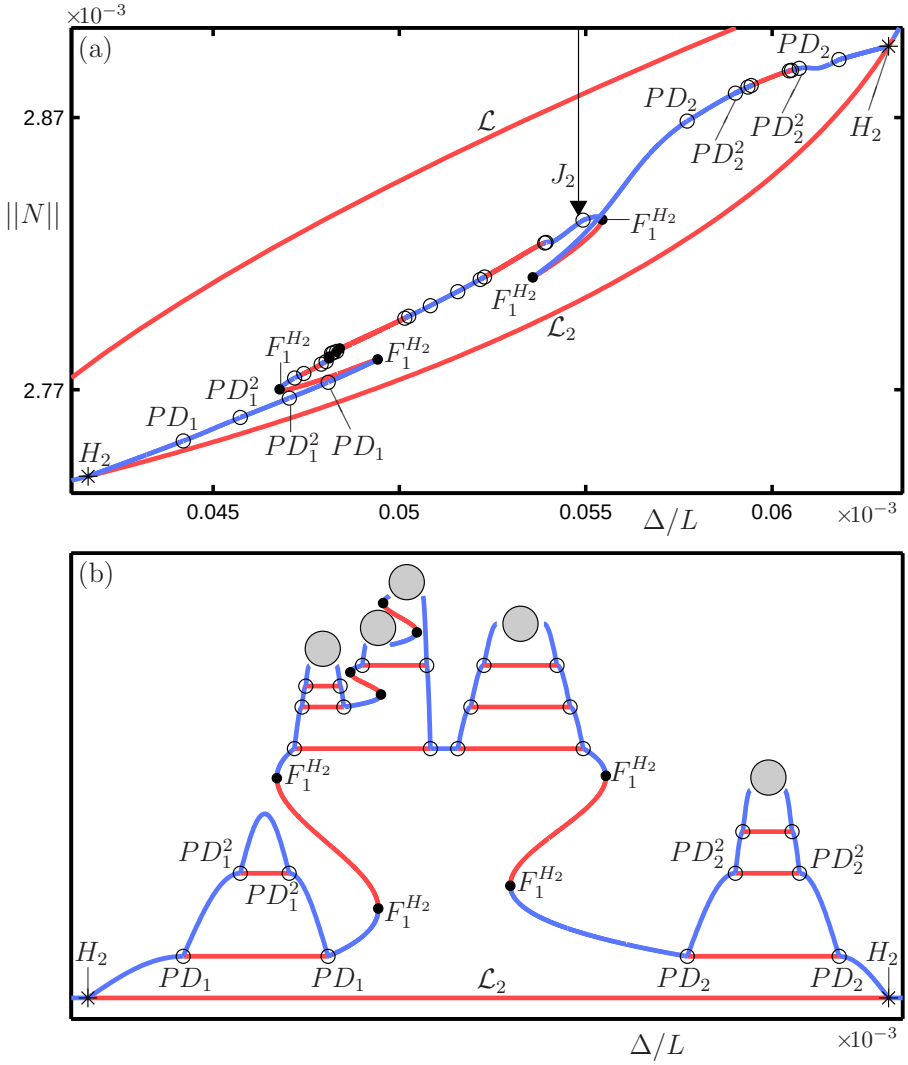

Fig. 15. One-parameter bifurcation diagram in Δ/L of the periodic solutions bifurcating from the coupled (Z_2, Y_2)-response of (4) for $\Omega/\omega_2 = 1.013$. Panel (a) shows the solutions in terms of $||N||$, and panel (b) is a schematic of the bifurcation diagram of the different branches of periodic orbits that were computed. Here open circles denote period-douling bifurcations and the large grey-filled circles indicate more complicated dynamics.

In order to investigate the corresponding cable dynamics with varying amplitudes of the contributing basic modes, we first continue the periodic orbits of the averaged equations (4). We then identify and confirm with simulations of the full Warnichai equations (1) that the corresponding cable dynamics indeed exists.

4.1. *Periodic orbits bifurcating from $\mathcal{L}_2$ for $\Omega/\omega_2 = 1.013$*

Figure 15 shows the corresponding bifurcation diagram of the periodic orbits of the averaged equations (4) that bifurcate from the branch $\mathcal{L}_2$ of the coupled (Z_2, Y_2)-response for $\Omega/\omega_2 = 1.013$. Panel (a) shows the branches of periodic orbits in terms of their norm $||N||$; compare with Fig. 14(b). Since these branches are so close to each other that it is difficult to distinguish them, Fig. 15(b) presents a schematic where the vertical axis shows an artificial norm that distinguishes the various solution branches; here the Δ/L axis remains unaltered to allow for a direct comparison with Fig. 15(a). Between the pair of Hopf bifurcation points labelled H_2 on the branch $\mathcal{L}_2$ of the coupled (Z_2, Y_2)-response there is a single branch of periodic orbits; we refer to it as the branch of basic periodic (Z_2, Y_2)-response. On this branch we find two pairs of fold bifurcations $F_1^{H_2}$ (saddle-node bifurcations of the periodic orbits), which lead to two regions of

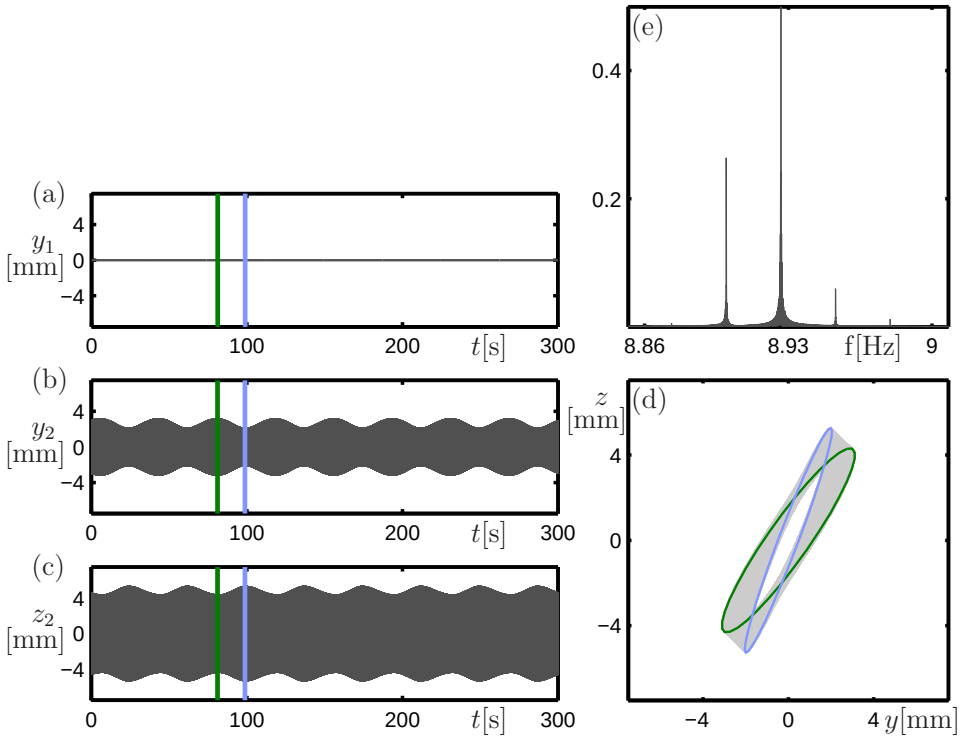

Fig. 16. Quasi-periodic cable dynamics of (1) with a period-one modulation of the amplitudes of z_2 and y_2, for $\Omega/\omega_2 = 1.013$ and $\Delta/L = 0.043 \times 10^{-3}$. The blue and green curves in panels (a)–(d) indicate two different basic periods of the response.

multistability between two different periodic (Z_2, Y_2)-responses. Moreover, we find two pairs of period-doubling bifurcations, inbetween which the basic branch of periodic (Z_2, Y_2)-response is unstable. We continued the period-doubled periodic orbits associated with these and several further period-doublings. Notice that the respective branches of periodic orbits are extremely close together in the $||N||$-projection; see Fig. 15(a) and (b). Overall, we found evidence of cascades of period-doublings that bound four regions with more complicated and potentially chaotic dynamics; these are indicated in Fig. 15(b) by large, grey-filled circles. Numerical simulations of (4) confirmed that the sequences of period-doubling bifurcations indeed lead to a chaotic attractor.

4.2. *Observed solutions of the Warnichai equations for* $\Omega/\omega_2 = 1.013$

We now shows that the averaged equations (4) correctly represent the cable dynamics as described by the full Warnichai equations (1), even on the level of solutions with varying amplitudes of the second in-plane mode Z_2 and the second out-of-plane mode Y_2. Firstly, a periodic solution of (4) corresponds to two-frequency dynamics of (1), where the underlying periodic cable dynamics at the basic frequency ω_2 is modulated in its amplitude. This two-frequency dynamics takes place on an invariant torus, and it may be quasi-periodic (so that it never repeats) or locked (so that it repeats after a number of basic periods). Similarly, a chaotic solution of (4) corresponds to chaotic dynamics of (1) with a chaotic modulation of the amplitude of the basic frequency. Specifically, the dynamics of (1) in z_2 and y_2 are coupled and their amplitudes are modulated, and we refer to a single oscillation in z_2 and y_2 as a basic period of the response.

Throughout, we generate an initial condition from the averaged equations (4) to start the simulation of the full Warnichai equations (1) and then record the result after transients died down (we typically discard at least the first 7,000 s). We then represent the observed dynamics in figures with five individual panels. Panels (a)–(c) show time series of y_1, y_2 and z_2, respectively, and panel (d) shows the corresponding trace of the quarter-span motion in the (y, z)-plane; compare with Fig. 13. Finally, panel (e) shows the

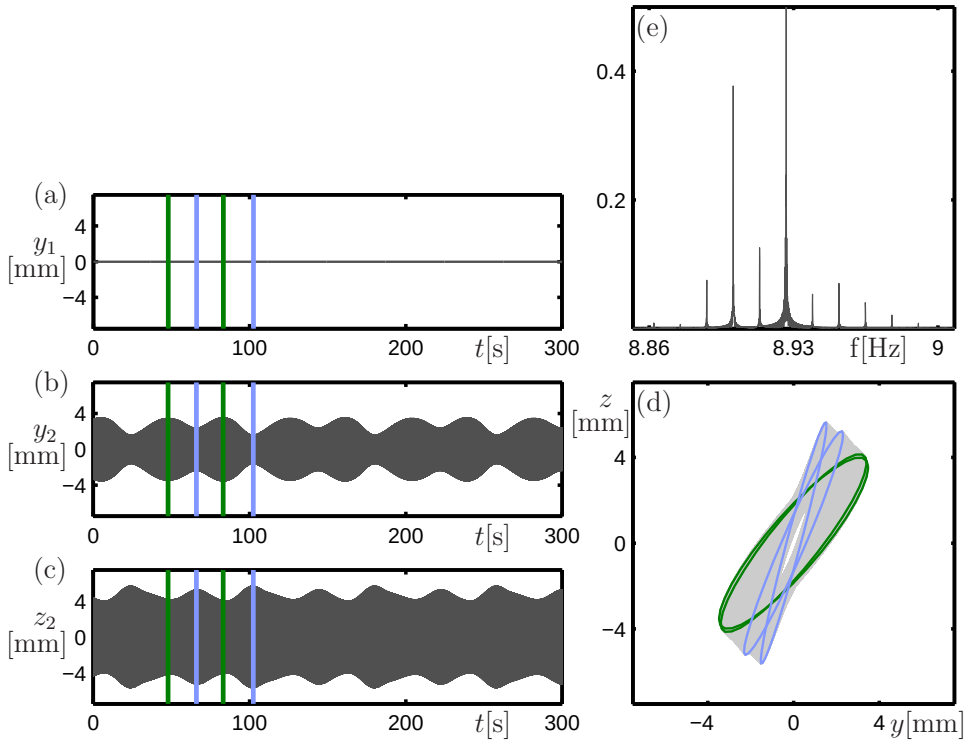

Fig. 17. Quasi-periodic cable dynamics of (1) with a period-two modulation of the amplitudes in z_2 and y_2, for $\Omega/\omega_2 = 1.013$ and $\Delta/L = 0.045 \times 10^{-3}$. The blue and green curves in panels (a)–(d) indicate four different basic periods of the response.

normalised frequency spectrum of the dynamics of y_2, as obtained by Fourier transform from long time series (of 7,000 s); it differentiates well periodic, quasi-periodic and chaotic cable motion.

Figure 16 shows the two-frequency cable dynamics of (1) that corresponds to the basic stable periodic orbit of (4), in between the bifurcations H_2 and PD_1 for $\Delta/L = 0.043 \times 10^{-3}$ in Fig. 15. In Fig. 16(a)–(c) the time series are plotted over a long time window of 300 s. Panel (a) confirms that the variable y_1 is inactive, and panels (b) and (c) show that the main oscillation of both z_2 and y_2 is modulated with a secondary slow frequency. Notice that the modulation of y_2 is out-of-phase with that of the z_2. Panel (d) shows the corresponding trace of the quarter-span motion in the (y, z)-plane, where the motion sweeps out a torus (grey area). Moreover, we also show two basic periods, one associated with the maximum (green curve) and one with the minimum of the y_2-modulation (blue curve). These two (almost) closed curves 'bound' the torus in Fig. 16(d); the corresponding times are shown by the two vertical lines in the time series in panels (a)–(c). Note that, at this scale, the fast underlying oscillation is not resolved in Fig. 16(a)–(d). Finally, the spectrum of the second out-of-plane y_2-response clearly shows beating peaks of the slower 0.026 Hz modulating frequency, which appear symmetrically on the left and the right of the main 8.926 Hz frequency peak (of the basic, fast oscillation). We conclude that the cable dynamics is quasi-periodic for all practical purposes; indeed it might be locked with an extremely high period, but these two scenarios are effectively indistinguishable.

Figure 17 shows the two-frequency cable dynamics of (1) that corresponds to the stable period-doubled orbit of (4), in between the bifurcations PD_1 and PD_2 for $\Delta/L = 0.045 \times 10^{-3}$ in Fig. 15. Figure 17 (b) and (c) clearly shows that the modulation has doubled in period, with two different local maxima and minima of the y_2-modulation in each period, examples of which are again highlighted as green and blue lines. They appear as (almost) closed curves in the quarter-span trace in the (y, z)-plane, where they again 'bound' the corresponding torus (grey area); see panel (d). The frequency spectrum in Fig. 17(e) clearly displays additional peaks, corresponding to a 0.013 Hz oscillation, which is half the modulation frequency of the period-one case; compare with Fig. 16(e). Overall, Fig. 17 demonstrates that we are dealing again

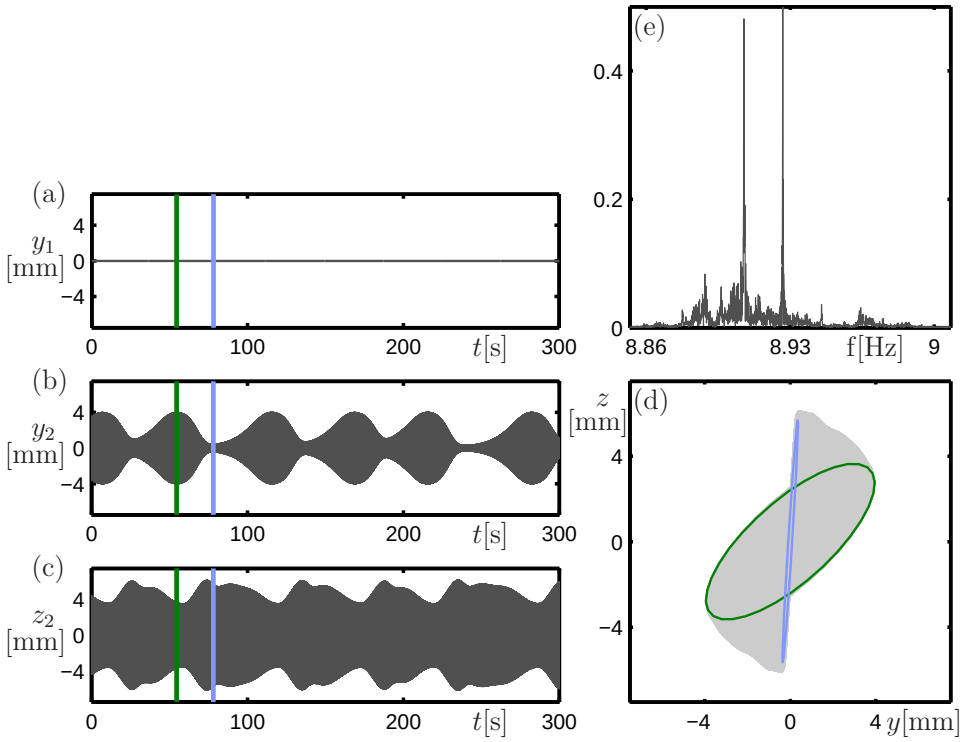

Fig. 18. Chaotic cable dynamics of (1) with a chaotic modulation of the amplitudes in z_2 and y_2, for $\Omega/\omega_2 = 1.013$ and $\Delta/L = 0.049 \times 10^{-3}$. The blue and green curves in panels (a)–(d) indicate two different basic periods of the response.

with quasi-periodic cable dynamics, but now on a doubled torus.

Finally, Fig. 18 illustrates chaotic cable dynamics of (1), which corresponds to chaotic amplitude dyanmics of (4) for $\Delta/L = 0.049 \times 10^{-3}$ in Fig. 15. The amplitude modulation in Fig. 18(b) and (c) does not appear to repeat, and notice from panel (a) that the y_1-response remains zero. The quarter-span trace in panel (d) still sweeps out an entire area (grey), that is still 'bounded' by two basic periods at a maximum (green curve) and a minimum of the y_2-modulation, respectively. The fact that this swept-out area is no longer the projection of a torus is comfirmed by Fig. 18(e): the frequency spectrum of y_2 still features the dominant fast oscillation peak at 8.926 Hz, but it is a now broad spectrum with effectively all other frequencies involved. This clearly demonstrates that the cable response is indeed chaotic.

4.3. *Influence of Ω/ω_2 and Shilnikov homoclinic bifurcation*

Figure 19 presents one-parameter bifurcation diagrams with the branches of the periodic (Z_2, Y_2)-solutions of (4) for $\Omega/\omega_2 = 1.0125$, again for 1.013, and for 1.0158, respectively. In panel (a) for $\Omega/\omega_2 = 1.0125$ the basic branch of periodic solutions connects the two Hopf bifurcation points, labelled H_2, on the steady-state branch $\mathcal{L}_2$. We find period-two solutions branches between the pairs of period-doubling points PD_1 and PD_2, and period-four solutions between the pair of further period-doublings PD_1^2. The unstable solutions are again so close to the stable branches that they cannot be distinguished in Fig. 19(a). Overall, the system follows the respective stable parts of the branches of period-one, period-two and pariod-four solutions as Δ/L is varied. In particular, there are no regions of chaotic dynamics for $\Omega/\omega_2 = 1.0125$. When Ω/ω_2 is increased to $\Omega/\omega_2 = 1.013$ as in Fig. 19(b), we find the branches of periodic orbits (now over a wider Δ/L-range) that were discussed in Sec. 4.1. These branches look very similar to those in Figure 19(a) in this projection but, as we have seen, for $\Omega/\omega_2 = 1.013$ there are fold bifurcations of periodic orbits and regions of chaotic cable dynamics. When Ω/ω_2 is increased even further to $\Omega/\omega_2 = 1.0158$ as in Fig. 19(c), there is no longer a single branch of periodic orbits that connects the two points of Hopf bifurcation H_2.

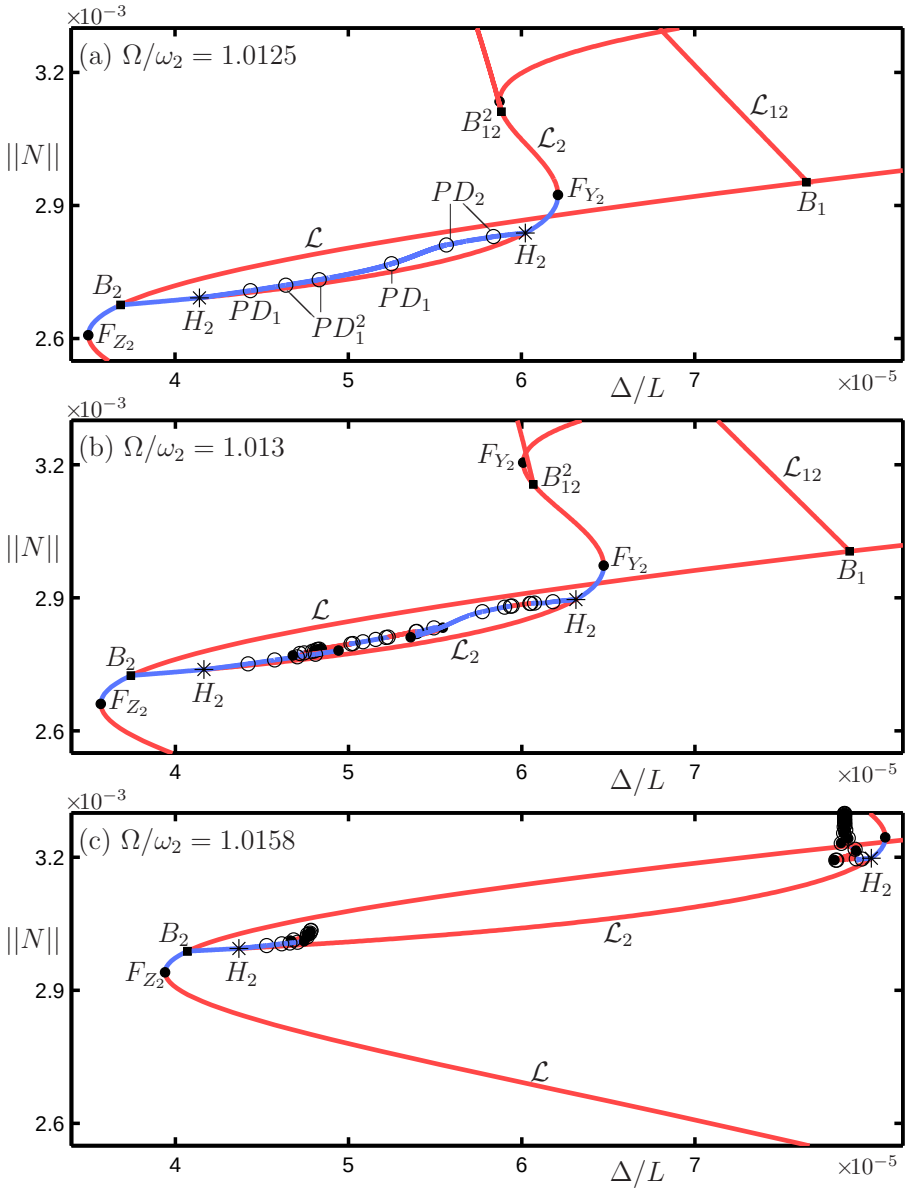

Fig. 19. One-parameter bifurcation diagrams in Δ/L of the periodic solutions bifurcating from the coupled (Z_2, Y_2)-response of (4) for $\Omega/\omega_2 = 1.0125$ (a), for $\Omega/\omega_2 = 1.013$ (b), and for $\Omega/\omega_2 = 1.0158$ (c).

Instead, we find distinct branches of periodic orbits near each of these two points, which appear to approach specific values of Δ/L.

Figure 20 shows enlarged views of these two branches of periodic solutions of (4). Panel (a) shows the branch bifurcating from the Hopf bifurcation point on $\mathcal{L}_2$ with the lower value of Δ/L. It shows a number of fold points, followed by period-doubling bifurcations, with sections of stable periodic orbits. The branch is eventually stable and appears to approach a specific value of Δ/L; at the same time, the period of the periodic solution tends to infinity. This is indicative of a Shilnikov homoclinic bifurcation, where the periodic orbit approaches a saddle focus [Guckenheimer & Holmes, 1996; Kuznetsov, 1998; Shilnikov, 1970; Shilnikov & Shilnikov, 2007]. For the Δ/L-value corresponding to the the very top of the branch shown in Fig. 20(a) we computed the four eigenvalues of the equilibrium of (4) that are associated with the two active modes z_2 and y_2 as $\lambda_{1,2} = -0.1107 \pm 0.3180i$, $\lambda_3 = 0.0275$ and $\lambda_4 = -0.2489$. This shows that the equilibrium is a saddle focus with a saddle index of $|Re(\lambda_1, 2)|/\lambda_3 > 1$; note that λ_4 is an additional, universally stronger attracting direction. We conclude that we are dealing with the case

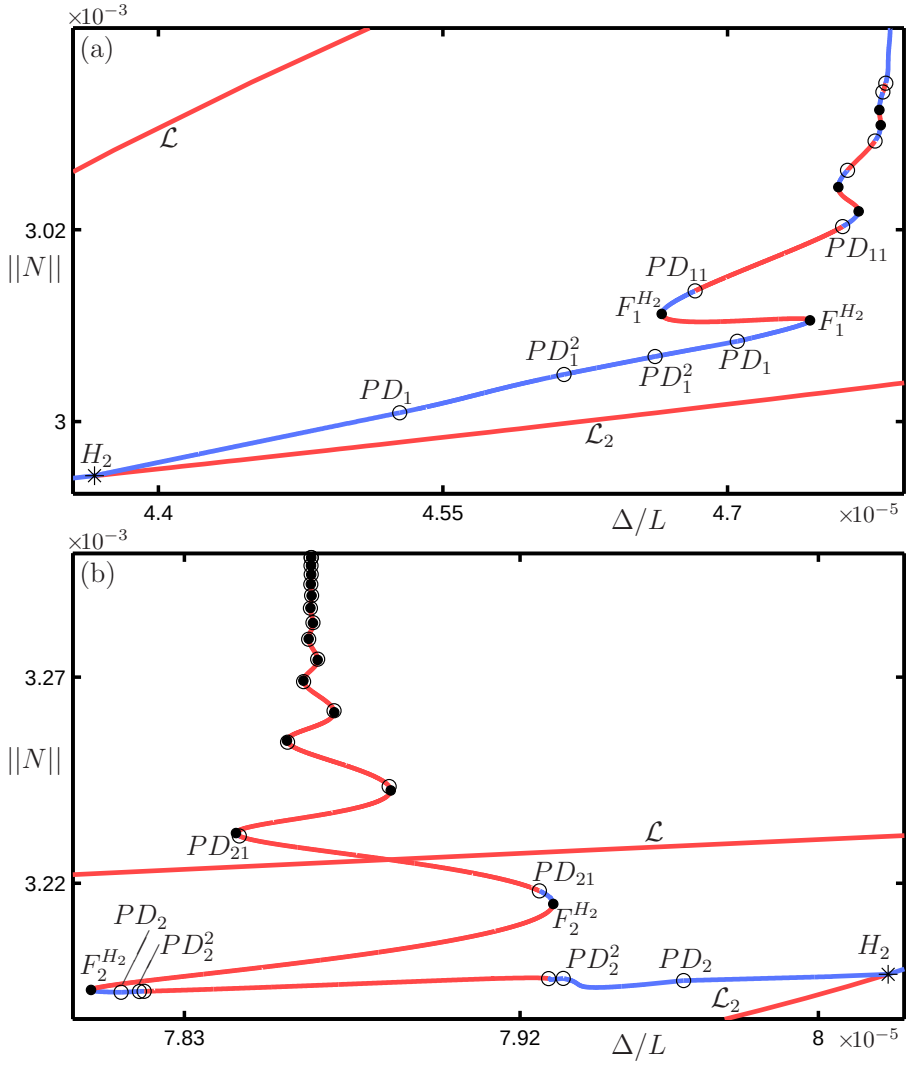

Fig. 20. Enlargements of the two branches of periodic solutions emerging from the Hopf bifurcation points on $\mathcal{L}_2$ of (4) for $\Omega/\omega_2 = 1.0158$, for lower (a) and higher (b) values of Δ/L; compare with Fig. 19(c).

of a simple Shilnikov bifurcation [Shilnikov, 1970; Shilnikov & Shilnikov, 2007], where a branch of stable periodic orbits approaches the saddle focus to become a homoclinic orbit.

Similarly, Fig. 20(b) near the Hopf bifurcation point on $\mathcal{L}_2$ with the higher value of Δ/L is indicative of another Shilnikov bifurcation, but now the branch of periodic solutions is largely unstable. The eigenvalues of the equilibrium (associated with z_2 and y_2) are $\lambda_{1,2} = -0.1107 \pm 0.5661i$, $\lambda_3 = 0.1396$ and $\lambda_4 = -0.3610$. Hence, we are again dealing with a saddle focus with an additional strong stable direction, but now with a saddle index of $|Re(\lambda_1)|/\lambda_3 < 1$. This means that the conditions for a chaotic Shilnikov orbit are satisfied [Shilnikov, 1970; Shilnikov & Shilnikov, 2007]. Note that the chaotic dynamics that arises due to this bifurcation is of saddle type, that is, unstable; in the respective range of Δ/L, we find that the dynamics of (4) settles down to the branch $\mathcal{L}$ of the directly excited pure Z_2-response.

As we show now, the Shilnikov bifurcation is indeed relevant for the observed cable dynamics. Figure 21 shows the cable response of the full Warnichai equations (1) for $\Omega/\omega_2 = 1.0158$ and $\Delta/L = 4.786 \times 10^{-5}$, which corresponds to the stable periodic orbit of (4) in Fig. 20(a) when it is very close to undergoing a (simple case of) Shilnikov bifurcation. The cable response is quasi-periodic (or of extremely high period), but observe from Fig. 21(b) and (c) that the modulation of the fast underlying oscillation is now very deep and anharmonic. Indeed, the frequency spectrum in Fig. 21(e) confirms the two-frequency nature of the

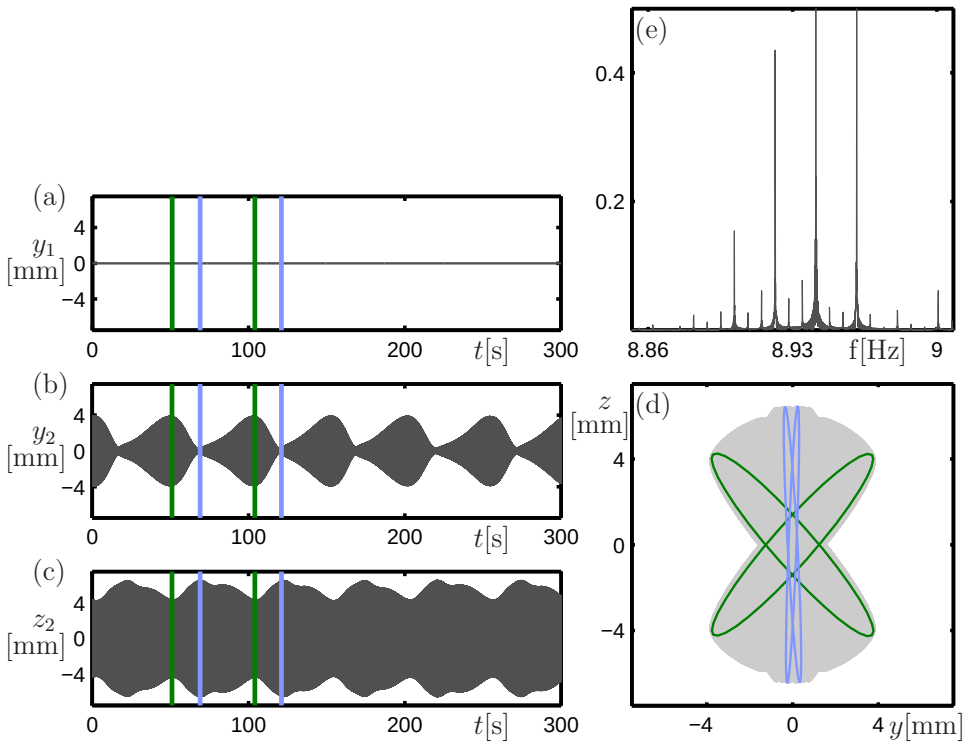

Fig. 21. Quasi-periodic cable dynamics of (1) for $\Omega/\omega_2 = 1.0158$ and $\Delta/L = 4.786 \times 10^{-5}$, corresponding to a stable periodic orbit of (4) close to the Shilnikov homoclinic bifurcation. The blue and green curves in panels (a)–(d) indicate four different basic periods of the response.

dynamics. An important observation from panel (d) is that the quarter-span trace is now symmetric with respect to the y-axis. In other words, the previously found two symmetrically related solutions of clockwise and counter-clockwise whirling motion of the cable have now merged. This means that the fast oscillation changes between being in-phase and being anti-phase over the course of two periods of the modulation, which corresponds to a change between clockwise and counter-clockwise whirling. This is illustrated in Fig. 21(d) by the fact that the green and blue traces of one basic period at consecutive maxima and minima of y_2 are each other's symmetric counterparts.

When Δ/L is increased very slightly, just past the Shilnikov bifurcation to $\Delta/L = 4.856 \times 10^{-5}$, the response of the cable as described by the full Warnichai equations (1) is as shown in Fig. 22. The modulation of the fast underlying oscillation is now no longer periodic; see panels (b) and (c). Rather we find extended periods over which the out-of-plane y_2-component is stronly suppressed; hence, the cable appears to be performing in-plane motion. However, the out-of plane motion then builds up to considerable values at irregular, unpredictable moments in time. The chaotic nature of the dynamics is confirmed by the frequency spectrum in panel (e), which shows a broad spectrum with several strong contributions from different frequencies. In spite of this change in dynamics, the quarter-span trace in Fig. 22(d) is still symmetric with respect to the y-axis. The green and blue traces of one basic period at consecutive maxima and minima of y_2 illustrate again that the fast oscillation still changes from being in-phase to being anti-phase, and back again. Hence, the cable motion changes irregularly between clockwise and counter-clockwise chaotic whirling.

We remark that a Shilnikov homoclinic bifurcation with positive saddle index was found by [Bajaj & Johnson, 1992] in a horizontal vibrating string upon variation of the frequency detuning parameter. They found the associated stable periodic dynamics and mention that no recurrent response is expected past the simple case of the Shilnikov bifurcation. Moreover, these authors observed the merging of two reflectionally symmetric orbits into a single symmetric orbit [Bajaj & Johnson, 1992; Johnson & Bajaj, 1989]. Our results

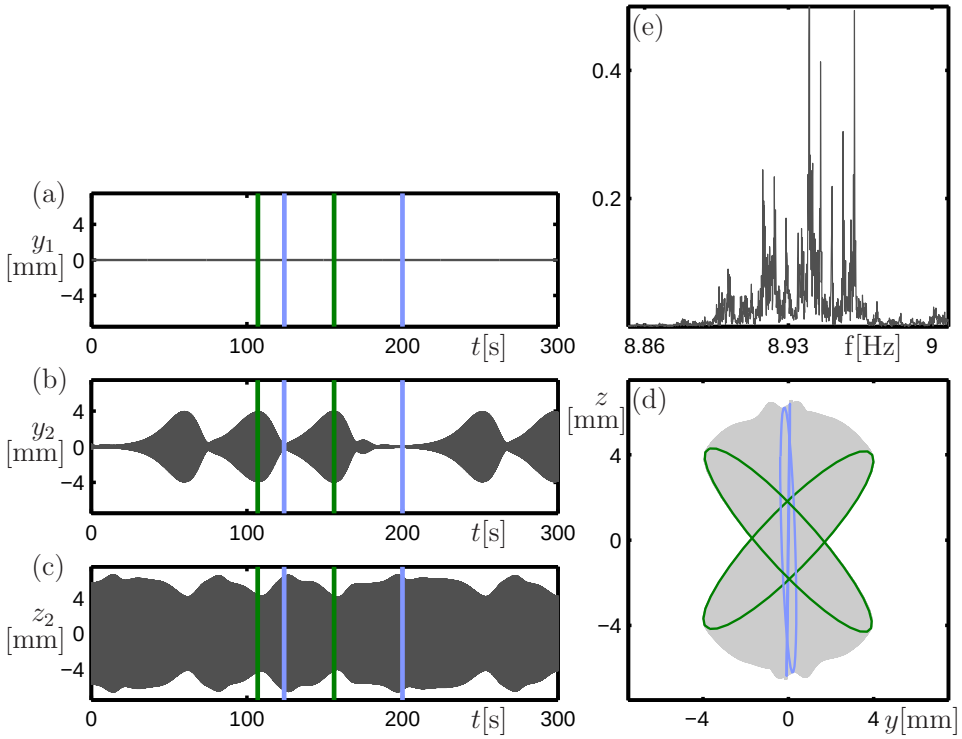

Fig. 22. Chaotic cable dynamics of (1) for $\Omega/\omega_2 = 1.0158$ and $\Delta/L = 4.856 \times 10^{-5}$, close to the Shilnikov homoclinic bifurcation of (4). The blue and green curves in panels (a)–(d) indicate four different basic periods of the response.

are very similar, but they are for an inclined cable, which differs from a horizontal string by the presence of a plane of inclination and the associated specific difference between in-plane and out-of-plane motion — not to mention the differences in parameter values between a string and a bridge cable. As we have seen, Figs. 21 and 22 clearly demonstrate that the Warnichai equations (1) have a complex whirling cable solution that undergoes a transition that corresponds directly to the Shilnikov homoclinic bifurcation of the averaged equations (4).

4.4. *Bifurcation diagram of periodic solutions in the $(\Omega/\omega_2, \Delta/L)$-plane*

The bifurcations of periodic orbits of the averaged equations (4) that were identified in Fig. 19 can be continued in two parameters in the $(\Omega/\omega_2, \Delta/L)$-plane. Figure 23 shows the resulting bifurcation diagram. Specifically, shown are the Hopf bifurcation curve H_2 (grey) with further bifurcations of periodic orbits that occur in the region to the right of H_2. For clarity, the different bifurcation curves are show in two panels. Figure 23(a) shows the first period-doubling curves PD_1 and PD_2 (red), second period-doubling curves PD_1^2 and PD_2^2 (blue), and the fold curves $F_1^{H_2}$ and $F_2^{H_2}$ (black). Figure 23(b) shows the curves PD_{11} and PD_{21} (blue) of period-doubling of periodic orbits that are created at $F_1^{H_2}$ and $F_2^{H_2}$, respectively; also shown is the curve $\mathscr{S}$ of Shilnikov homoclinic bifurcations, which was continued in two parameters as a periodic orbit of sufficiently large period.

Figure 23 shows how the one-parameter bifurcation diagram in Δ/L becomes more complicated when Ω/ω_2 is increased. The dashed vertical lines mark the cross sections where Ω/ω_2 takes the values 1.0125, 1.013 and 1.0158. Hence, the crossing points of these lines with the different bifurcation curves yield the respective bifurcations in the one-parameter bifurcation diagrams of Figs. 14, 15, 19 and 20. Regions with chaotic dynamics of (4) can be found only for sufficiently large Ω/ω_2 when there is a full period-doubling sequence to chaos for lower and/or larger values of Δ/L; this happens only after the curves PD_1^2 and PD_2^2 are intersected, respectively. For sufficiently large Ω/ω_2 the curves $F_1^{H_2}$ or $F_2^{H_2}$ in Fig. 23(a) are crossed at

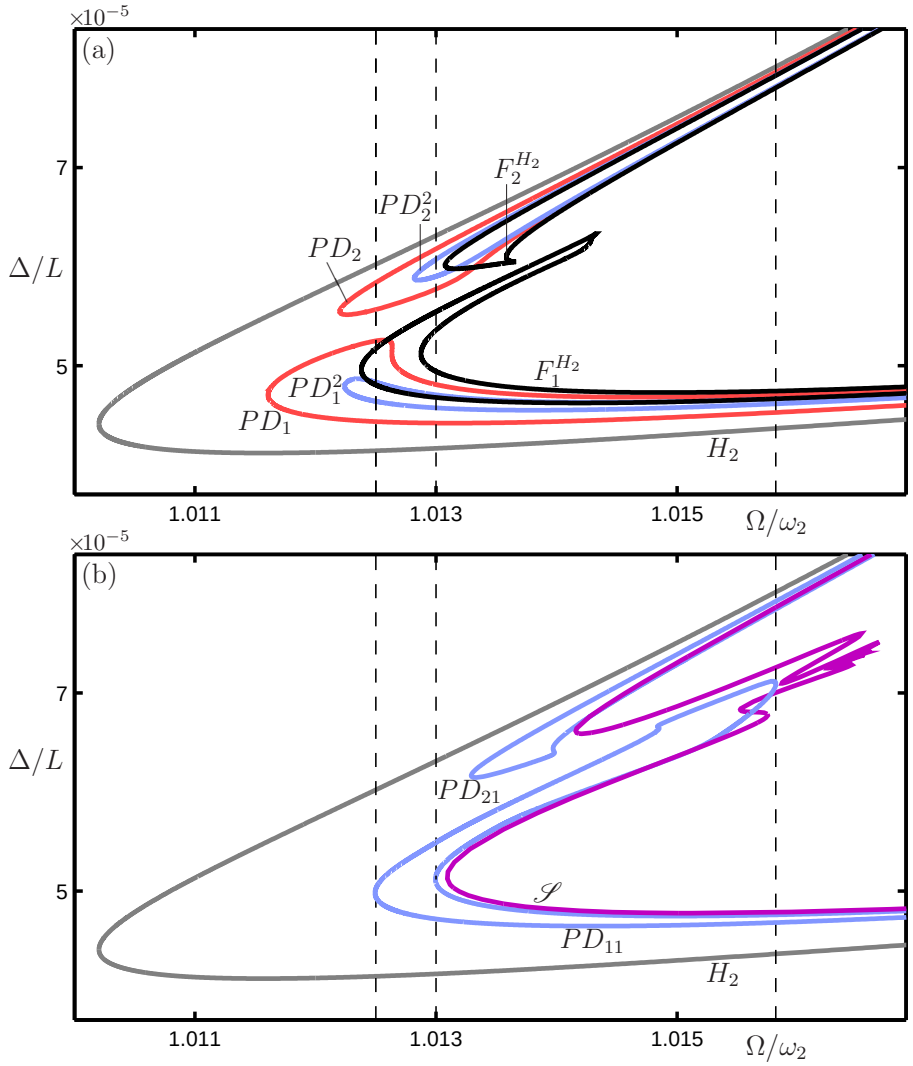

Fig. 23. Two-parameter bifurcation diagram in the $(\Omega/\omega_2, \Delta/L)$-plane of the periodic (Z_2, Y_2)-solutions of the averaged equtions (4). Panel (a) shows the loci H_2 (grey) of Hopf bifurcations, PD_1 and PD_2 (red) of first period-doubling, PD_1^2 andPD_2^2 (blue) of second period-doubling, and $F_1^{H_2}$ and $F_2^{H_2}$ (black) of fold bifurcations of periodic orbits. Panel (b) shows the loci H_2 (grey) of Hopf bifurcations, PD_{11} and PD_{21} (blue) of period-doubling, and $\mathscr{S}$ (purple) of Shilnikov homoclinic bifurcations. The dashed vertical lines correspond to the one-parameter bifurcation diagrams in Fig. 19.

least twice when Δ/L is increased or decreased, and this leads to hysteresis loops. Notice that the dashed vertical line for $\Omega/\omega_2 = 1.0125$ crosses the boomerang-shaped curve $F_1^{H_2}$ and in a way that implies that there is an isolated branch of periodic solutions. It is not shown here, but we remark that such an isolated branch was also found for a vibrating horizontal string in [Bajaj & Johnson, 1992; Johnson & Bajaj, 1989]. The bifurcating periodic solutions undergo period-doubling at the curves PD_{11} and PD_{21} shown in Fig. 23(b). Notice further that one finds a Shilnikov homoclinic bifurcation and associated dynamics in the one-parameter diagram in Δ/L only for sufficiently large Ω/ω_2, when the respective parts of the curve $\mathscr{S}$ are intersected by the corresponding vertical line. Along the part of $\mathscr{S}$ for lower values of Δ/L the saddle index is greater than one, and along the part of $\mathscr{S}$ for larger values of Δ/L the saddle index is smaller than one; compare with Fig. 20.

Even though we chose here to present one-parameter bifurcation diagrams in Δ/L for fixed Ω/ω_2, Fig. 23 shows how the respective regions of complex cable response arise when Ω/ω_2 is varied for fixed Δ/L. For example, the part of $\mathscr{S}$ with saddle index greater than one can be reached by increasing Ω/ω_2 for a suitable value of Δ/L; this choice of free parameter was used in [Bajaj & Johnson, 1992; Molteno &

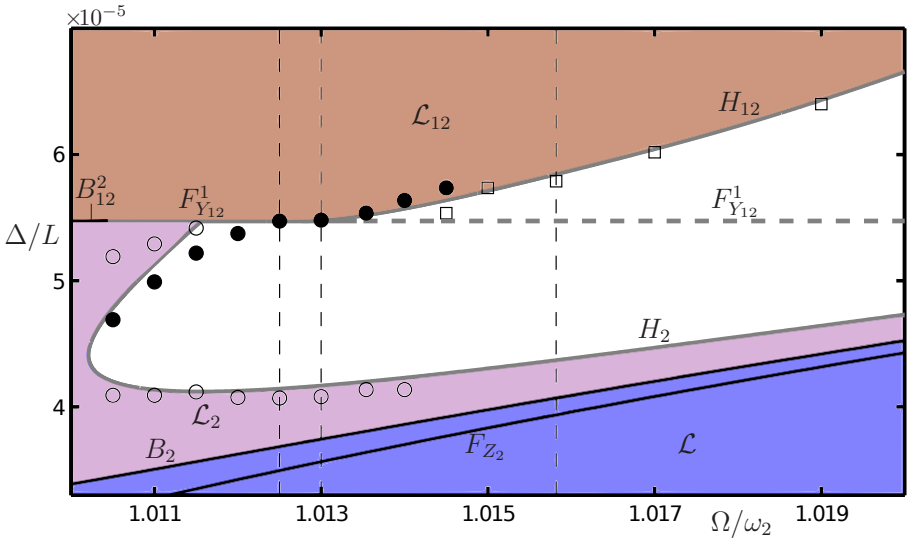

Fig. 24. Changes of the cable response in the $(\Omega/\omega_2, \Delta/L)$-plane found in simulations of the Warnitchai equations (1) that start from the (Z_2, Y_2, Y_1)-response and ramp down Δ/L: filled circles indicate a transition to a quasi-periodic (Z_2, Y_2)-response, while circles and squares represent transitions to a coupled (Z_2, Y_2)-response and to a pure Z_2-response, respectively. Shown for comparison are the regions of stability of the modes $\mathcal{L}$ (blue shading), $\mathcal{L}_2$ (purple shading) and $\mathcal{L}_{12}$ (brown shading) of the averaged equations (4), and the bifurcation curves H_2, B_2, F_{Z_2}, B^2_{12}, $F^2_{Y_{12}}$ and H_{12}. The dashed vertical lines correspond to the one-parameter bifurcation diagrams in Fig. 19.

Tufillaro, 1990; O'Reilly & Holmes, 1992] in the investigation of dynamics associated with the Shilnikov homoclinic orbit in the model of a horizontal string.

We now consider where in the $(\Omega/\omega_2, \Delta/L)$-plane one finds transitions of the full Warnitchai equations (1) to a varying-amplitude response. To this end, we perform simulations of (1) for fixed Ω/ω_2 and starting on the branch $\mathcal{L}_{12}$ of a harmonic, fixed amplitude (Z_2, Y_2, Y_1)-response. As one would do in an experiment, we then track the observed solution when Δ/L is slowly ramped down. Transitions to a quasi-periodic (Z_2, Y_2)-response, to a harmonic (Z_2, Y_2)-response and to a harmonic Z_2-response are detected in the time series.

Figure 24 shows the recorded transitions of the Warnitchai equations (1) in the $(\Omega/\omega_2, \Delta/L)$-plane as filled circles, circles and squares, overlaid onto the stability diagram of the underlying equilibrium solutions of the averaged equations (4); compare with Sec. 3.5. Specifically, shown are the projections of the stable parts of the solution surfaces $\mathcal{L}$ (blue shading), $\mathcal{L}_2$ (purple shading) and $\mathcal{L}_{12}$ (brown shading) from Fig. 10; here, the stability region of $\mathcal{L}_{12}$ is shown 'on the top', because all simulations start from the stable pure (Z_2, Y_2, Y_1)-response. Also shown are corresponding bifurcation curves. The curves B^2_{12} and H_2 are shown only until they go 'underneath' the stable part of $\mathcal{L}_{12}$. Both $F^1_{Y_{12}}$ and H_{12} belong to $\mathcal{L}_{12}$, where $F^1_{Y_{12}}$ arises from B^2_{12} and H_{12} arises from $F^1_{Y_{12}}$. The part of $F^1_{Y_{12}}$ that corresponds to a fold of unstable (Z_2, Y_1, Y_2)-solutions is dashed. The results of the simulations of (1) are depicted as follows. Filled circles denote points where a quasi-periodic (two-frequency) (Z_2, Y_2)-response is detected for the first time, and open circles and squares denote first detection of a coupled (Z_2, Y_2)-response and a pure Z_2-response, respectively. Notice that the filled circles are aligned with the curves H_2, $F^1_{Y_{12}}$ and H_{12}, the open circles are aligned with H_2, and the squares are aligned with H_{12}.

The recorded transitions of the Warnitchai equations (1) in Fig. 24 correspond to the transitions shown in Fig. 14. As in Fig. 23, the dashed vertical lines correspond to the respective one-parameter bifurcation diagrams of Figs. 14, 15 19 and 20. Specifically for $\Omega/\omega_2 = 1.013$, the transition J_2 corresponds to the filled circle, and passing through the Hopf bifurcation H_2, just before J_3, corresponds to the open circle in Fig. 24. Overall, Fig. 24 shows how the dynamics of the cable changes from the coupled (Z_2, Y_2, Y_1)-response back to the pure Z_2-response as Δ/L is decreased. For $\Omega/\omega_2 \in [1, 1.01]$ only the harmonic oscillations of the coupled (Z_2, Y_2)-response appear before the cable goes back to the pure Z_2-response. For $\Omega/\omega_2 \in (1.01, 1.014]$ there

is a region of varying-amplitude quasi-periodic (Z_2, Y_2)-response, just as we found for $\Omega/\omega_2 = 1.013$. For $\Omega/\omega_2 \in (1.014, 1.0145]$ the quasi-periodic dynamics of the Warnichai equations suddenly loses stability and a transition to the pure modal Z_2-response occurs. For $\Omega/\omega_2 \in (1.0145, 1.02]$ there is a direct transition from the coupled (Z_2, Y_2, Y_1)-response to the pure Z_2-response.

Overall, we identified a region in the $(\Omega/\omega_2, \Delta/L)$-plane, where a quasi-periodic (Z_2, Y_2)-response of the inclined cable has been confirmed by simulations of the full Warnitchai equations (1) that started from a stable coupled (Z_2, Y_2, Y_1)-response and decreased Δ/L. The fact, that this region is bounded in very good approximation by corresponding bifurcation curves of the averaged equations (4) demonstrates not only its accuracy, but also the usefulness of the bifurcation theory approach taken in this paper.

5. Conclusions

We presented a bifurcation study of an inclined cable with support excitation near a 2 : 1 resonance with the second natural frequency of the cable. This system was modelled by the Warnitchai ODEs for the directly excited in-plane mode and for the first and second out-of-plane modes of the cable. We also considered the corresponding averaged system that describes only the amplitude dynamics of the three modes. Throughout the frequency range of forcing we considered, we found that the averaged equations provide an accurate description of the dynamics of the full Warnichai equations, also for cable responses with varying amplitudes; this can be explained by the fact that the observed modulation period of the amplitudes is much larger than the basic period of the forcing.

The first focus of our investigation was on the different types of coupled-mode, constant-amplitude responses of the inclined cable; these are equilibria of the averaged equations that are distinguished by which of the out-of-plane modes is active: none, the first, the second, or both. Each of the four types of equilibria was computed by means of numerical continuation as a surface in the three-dimensional space of their norm versus the amplitude and frequency of the excitation. The different surfaces connect at curves of bifurcations and constitute a geometric picture of the overall two-parameter bifurcation diagram of the coupled-mode response of the cable. In particular, this analysis identified several previously unknown branches of stable coupled-mode responses. The quite intricate structure of this bifurcation diagram and the associated stability regions of the different coupled modes confirms the nonlinear nature of the problem. In particular, we found that the frequency response of the cable depends very sensitively on the excitation amplitude.

Secondly, we studied bifurcating periodic solutions of the averaged equations, which correspond to varying-amplitude whirling responses of the inclined cable. We found several branches of stable periodic orbits. Moreover, we identified further bifurcations, including period-doublings and a Shilnikov homoclinic bifurcation, that lead to chaotic dynamics of the cable. These findings were presented as a bifurcation and stability diagram in the $(\Omega/\omega_2, \Delta/L)$-plane. Simulations confirmed that the corresponding varying-amplitude cable responses can indeed also be found in the full Warnitchai equations. The cable dynamics was represented by time series, quarter-span traces and frequency spectra.

The results we presented are for a range of the excitation frequency (close to the 2 : 1 resonance) where the first in-plane mode is not active and, therefore, the three-mode model considered here provides a suitable description of the cable response. While this amplitude and frequency range of the forcing looks quite small in the rescaled parameters used here, it is of relevance for the original problem of bridge cable vibration, and in line with the frequency ranges that have been considered in experiments as physically accessible. For example, the Warnichai model as considered here was studied in [Gonzalez-Buelga *et al.*, 2008] mainly in terms of the stability properties of the pure in-plane response, and good agreement was found with the corresponding experiment. Similar experiments are reported in [Marsico *et al.*, 2011] for a longer cable, where again there was good agreement between measurements and the stability boundaries of in-plane motion. These results were obtained for a four-mode model that includes the first in-plane mode; however, the stability boundaries agree with those of the three-mode model for frequency detunings as considered here. It appears feasible for these reasons that the cable responses predicted here, including whirling, quasi-periodic and chaotic cable responses, may also be confirmed experimentally. Note, however, that such experiments are not straightforward, because the cable is only very lightly damped. Hence,

experimental runs require a long time for transients to die down sufficiently before the dynamics can be recorded reliably (e.g., with video-capture at the half- and quarter-spans).

Finally, we mention that in a cable-stayed bridge the cable dynamics may also have an influence on the bridge deck. The study presented here shows that the motion of the cable itself, under uni-directional excitation from the deck, may develop considerable amplitudes. Hence, there is the potential for positive feedback between vibrations of the cable and the deck. One approach to studying such effects is to extend the model for the cable by adding one or more damped oscillators that model the basic modes of the bridge deck. This type of system could be studied in a similar spirit via a bifurcation analysis of the coupled-mode responses of the overall system, which now also includes the basic deck modes.

Acknowledgements

The research of V.T. was supported by grant EP/F030711/1 from the Engineering and Physical Sciences Research Council (EPSRC).

References

Bajaj, A. K. & Johnson, J. M. [1992] "On the amplitude dynamics and crisis in resonant motion of streched strings," *Phil. Trans. Royal Soc. London* **A 338**(1649), 1–41.

Berlioz, A. & Lamarque, C. H. [2005] "A non-linear model for the dynamics of an inclined cable," *J. Sound and Vibration*, **279**(3–5), 619–639.

Doedel, E. J., with major contributions from Champneys, A. R. Fairgrieve, T.F., Kuznetsov, Yu. A., Oldeman, B. E., Paffenroth, R. C. , Sandstede, B., Wang, X. J. & Zhang, C [2000] "AUTO2000 and AUTO-07P: Continuation and bifurcation software for ordinary differential equations," *Technical Report*, Department of Computer Science, Concordia University, Montreal, Canada; available from `http://sourceforge.net/projects/auto2000`.

Doedel E. J. [2007] in *Numerical Continuation Methods for Dynamical Systems*, edited by Krauskopf, B., Osinga, H.M. & Galán-Vioque, J., Springer-Verlag, Dordrecht, pp. 1–49.

Fujino, Y., Warnitchai P. & Pacheco, B. M. [1993] "An experimental and analytical study of autoparametric resonance in a 3DOF model of cable-stayed-beam," *Nonlinear Dynam.* **4**, 111–138.

Gattulli, V., Lepidi, M., Macdonald, J. H. G. & and Taylor, C. A. [2005] "One-to-two global local interaction in a cable stayed beam observed through analytical, finite element and experimental models, " *International Journal of Non-Linear Mechanics* **40**(5), 571–588.

Gattulli, V., Martinelli, L., Perotti, F. & Vestroni, F. [2004] "Non-linear oscillations of cables under harmonic loading using analytical and finite element models," *Comput. Meth. Appl. Mech. Eng.* **193**, 69–85.

Georgakis, C. T., Macdonald, J. H. G. & and Taylor, C. A. [2001] "Non-linear analysis of wind-induced cable-deck interaction," *IABSE Conference Cable-supported Bridges, Seoul, South Korea*, IABSE Reports **84**, Paper 330.

Gonzalez-Buelga, A., Neild, S. A., Wagg, D. J. & Macdonald, J. H. G. [2008] "Modal stability of inclined cables subjected to vertical support excitation," *J. Sound and Vibration* **318**, 565–579.

Guckenheimer, J. & Holmes P. [1986] *Nonlinear Oscillations, Dynamical Systems and Bifurcations of Vector Fields*, Springer-Verlag, New York/Berlin, second edition.

Irvine, H. [1981] *Cable structures*, MIT Press, Cambridge, MA.

Kirchhoff, G. [1883] *Vorlesungen über mathematische Physik*, Druck and Verlag von B. G. Teubner, Leipzig.

Kuznetsov, Yu. A. [1998] *Elements of Applied Bifurcation Theory*, Springer-Verlag, New York/Berlin, second edition.

Johnson, J. M. & Bajaj, A. K. [1989] "Amplitude modulated and chaotic dynamics in resonant motion of string," *J. Sound and Vibration* **128**, 87–107.

Lilien, J. L. & Pinto Da Costa, A. P.[1994] "Vibration amplitudes caused by parametric excitation of cable stayed structures," *J. Sound and Vibration* **174**, 69–90.

Macdonald, J. H. G., Dietz, M. S., Neild, S. A., Gonzalez-Buelga, A., Crewe, A. J. & Wagg, D. J. [2010]

"Generalised modal stability of inclined cables subjected to support excitations," *J. Sound and Vibration* **329**, 4515–4533.

Marsico, M. R., Tzanov, V., Wagg, D. J., Neild, S. A. & Krauskopf, B. [2011] "Bifurcation analysis of a parametrically excited inclined cable close to two-to-one internal resonance," *J. Sound and Vibration* **330**, 6023–6035.

Miles, J. [1984] "Resonant, nonplanar motion of a streched string," *J. Acoust. Soc. America* **75**, 1505–1510.

Molteno, T. & Tufillaro, N. [1990] "An experimental investigation into the dynamics of a string," *Americ. J. Physics* **72**, 1157–1169.

Molteno, T. & Tufillaro, N. [1990] "Torus doubling and chaotic string vibrations: experimental results," *J. Sound and Vibration* **137**, 327–330.

Narashima R. [1968] "Nonlinear vibration of an elastic string," *J. Sound and Vibration* **8**, 134–146.

Nayfeh, A. H. & Pai, P. F. [2004] *Linear and Nonlinear Structural Mechanics*, Wiley.

O'Reilly, O. & Holmes, P. [1992] "Non-linear, non-planar and non-periodic vibrations of a string," *Journal of Sound and Vibration* **153**(3), 413–435.

Rega, G. [2004] "Nonlinear vibrations of suspended cables- part i: Modeling and analysis," *Applied Mechanics Review* **57**, 443–478.

Rega, G. [2004] "Nonlinear vibrations of suspended cables- part ii: Deterministic phenomena," *Applied Mechanics Review* **57**, 479–514.

Rega, G., Alaggio, R. & Benedettini, F. [1997] "Experimental investigation of the nonlinear response of a hanging cable. part I: Local analysis," *Nonlinear Dynamics* **17**, 89–117.

Rega, G. & Alaggio, R. [2009] "Experimental unfolding of the nonlinear dynamics of a cable-mass suspended system around a divergence-Hopf bifurcation," *J. Sound and Vibration* **322**, 581–611.

Rega, G., Lacarbonara, W., Nayfeh, A. H. & Chin, C. M. [1999] "Multiple resonances in suspended cables: direct versus reduced-order models," *Int. J. Non-linear Mechanics* **34**(5), 901–924.

Rega, G., Srinil, N. & Alaggio, R. [2008] "Experimetal and numerical studies of inclined cables: free and parametrically-forced vibrations," *J. Theor. Appl. Mechanics*, **3**(46), 621–640.

Shilnikov, L. [1970] "A contribution to the problem of the structure of an extended neighborhood of a rough equilibrium state of saddle-focus type," *Math. USSR-Sbornik* **10**, 91–102.

Shilnikov, L. P. & Shilnikov, A. [2007] "Shilnikov bifurcation," *Scholarpedia* **2**(8), 1891.

Srinil, N. & Rega, G. [2007] "Two-to-one resonant multi-modal dynamics of horizontal/inclined cables. part ii: Internal resonance activation, reduced-order models and nonlinear normal modes," *Nonlinear Dynamics* **48**(3), 253–274.

Srinil, N., Rega, G. & Chucheepsakul, S. [2004] "Three-dimensional non-linear coupling and dynamic tension in the large-amplitude free vibrations of arbitrarily sagged cables," *J. Sound and Vibration* **269**(3-5), 823–852.

Srinil, N., Rega, G. & Chucheepsakul, S. [2007] "Two-to-one resonant multi-modal dynamics of horizontal/inclined cables. part i: Theoretical formulation and model validation," *Nonlinear Dynamics* **48**(3), 231–252.

Tagata, G. [1977] "Harmonically forced, finite amplitude vibration of a string," *J. Sound and Vibration* **51**(4), 483492.

Tzanov, V. [2012] "Bifurcation analysis applied to inclined cable dynamics," *PhD Thesis, University of Bristol, United Kingdom.*

Tzanov, V., Neild, S. A., Krauskopf, B. & Wagg, D. J. [2011] "Influence of damping on the vibration of an inclined cable subjected to support excitation," *Proceedings of ASME 2011 Design Engineering technical Conference and Computers and Information in Engineering Conference.*

Uhrig, R. [1993] "On kinetic response of cables of cable-stayed bridges due to combined parametric and forced excitation," *J. Sound and Vibration* **165**(1), 185192.

Wagg, D. J. & Neild, S. A. [2010] *Nonlinear Vibration with Control.* Springer-Verlag.

Warnitchai, P., Fujino, Y. & Susumpow, T. [1995] "A nonlinear dynamic model for cables and its application to a cable structure system," *J. Sound and Vibration* **187**(4), 695–712.